

Sibiriline, a new small chemical inhibitor of receptor-interacting protein kinase 1, prevents immune-dependent hepatitis

Fabienne Le Cann^{1,2,†}, Claire Delehouzé^{3,†}, Sabrina Leverrier-Penna^{1,2,†}, Aveline Filliol^{1,2}, Arnaud Comte⁴, Olivier Delalande⁵, Nathalie Desban³, Blandine Baratte³, Isabelle Gallais^{1,2}, Claire Piquet-Pellorce^{1,2}, Florence Faurez^{1,2}, Marion Bonnet^{1,2,6}, Yvette Mettey⁷, Peter Goekjian⁸, Michel Samson^{1,2}, Peter Vandenabeele^{9,10}, Stéphane Bach^{3,‡} and Marie-Thérèse Dimanche-Boitrel^{1,2,‡}

1 INSERM UMR 1085, l'Environnement et le Travail, Institut de Recherche sur la Santé, Rennes, France

2 Biosit UMS 3080, Université de Rennes 1, France

3 UPMC Univ Paris 06, CNRS USR3151, Protein Phosphorylation and Human Disease Laboratory, Sorbonne Universités, Roscoff, France

4 CNRS UMR 5246, Chimiothèque, ICBMS, Université Claude Bernard Lyon 1, Villeurbanne, France

5 CNRS UMR 6290, Institut de Génétique et Développement de Rennes, Université de Rennes 1, France

6 Division of Infection & Immunity, College of Biomedical and Life Sciences, Cardiff University, UK

7 Laboratoire Chimie Organique, Faculté de Médecine-Pharmacie, Laboratoire Signalisation et Transports Ioniques Membranaires, CNRS, Université de Poitiers, Poitiers Cedex, France

8 CNRS UMR 5246, Laboratoire Chimie Organique 2-Glycosciences, ICBMS, Université de Lyon, Université Claude Bernard Lyon 1, Villeurbanne, France

9 Molecular Signaling and Cell Death Unit, VIB Inflammation Research Center, Ghent, Belgium

10 Department of Biomedical Molecular Biology, Ghent University, Belgium

Keywords

Concanavalin A -induced hepatitis; kinase inhibitor; molecular docking; necroptosis; RIPK1 inhibitor

Correspondence

S. Bach, Protein Phosphorylation and Human Disease Laboratory, Station Biologique, Place Georges Teissier, F-29688 Roscoff, France

Fax: +33 2 98 29 25 26

Tel: +33 2 98 29 23 91

E-mail: bach@sb-roscoff.fr

and

M-T. Dimanche-Boitrel, INSERM UMR 1085, Institut de Recherche sur la Santé, Environnement et Travail, 2 avenue du Pr Léon Bernard, F-35043 Rennes, France

Fax: +33 2 23 23 47 94

Tel: +33 2 23 23 48 99

E-mail: marie-therese.boitrel@univ-rennes1.fr

[†]These authors contributed equally to this work

[‡]These authors share senior authorship

(Received 27 March 2017, revised 15 June 2017, accepted 13 July 2017)

doi:10.1111/febs.14176

Necroptosis is a regulated form of cell death involved in several disease models including in particular liver diseases. Receptor-interacting protein kinases, RIPK1 and RIPK3, are the main serine/threonine kinases driving this cell death pathway. We screened a noncommercial, kinase-focused chemical library which allowed us to identify Sibiriline as a new inhibitor of necroptosis induced by tumor necrosis factor (TNF) in Fas-associated protein with death domain (FADD)-deficient Jurkat cells. Moreover, Sib inhibits necroptotic cell death induced by various death ligands in human or mouse cells while not protecting from caspase-dependent apoptosis. By using competition binding assay and recombinant kinase assays, we demonstrated that Sib is a rather specific competitive RIPK1 inhibitor. Molecular docking analysis shows that Sib is trapped closed to human RIPK1 adenosine triphosphate-binding site in a relatively hydrophobic pocket locking RIPK1 in an inactive conformation. In agreement with its RIPK1 inhibitory property, Sib inhibits both TNF-induced RIPK1-dependent necroptosis and RIPK1-dependent apoptosis. Finally, Sib protects mice from concanavalin A-induced hepatitis. These results reveal the small-molecule Sib as a new RIPK1 inhibitor potentially of interest for the treatment of immune-dependent hepatitis.

Abbreviations

ALT, alanine aminotransferase; AST, aspartate aminotransferase; ATP, adenosine triphosphate; AU, arbitrary unit; DR, death receptor; FasL, Fas ligand; MD, molecular docking; MEFs, mouse embryonic fibroblasts; Nec-1, necrostatin-1; RT, room temperature; Sib-i, inactive Sibiriline; Sib, Sibiriline; TNF, tumor necrosis factor; TRAIL, TNF-related apoptosis-inducing ligand.

Introduction

Excessive hepatocyte cell death has been identified as a central pathophysiological mechanism in both acute and chronic liver injuries, involving mostly cell death by apoptosis and necrosis (oncosis) [1]. More recently, necroptosis, a specific form of regulated necrosis, has also been implicated in liver disease models [2,3]. Necroptosis is a caspase-independent nonapoptotic backup cell death mechanism initiated upon blockade of apoptosis [4]. This cell death pathway is dependent on serine/threonine receptor-interacting protein kinases, RIPK1 and RIPK3, and a pseudokinase MLKL (mixed-lineage kinase domain-like) (see for review [5]). Moreover, it is inhibited by necrostatin-1 (Nec-1), the first small tryptophan-based molecule inhibitor of RIPK1 kinase activity [4,6].

Necroptosis may occur in response to various stimuli [5]. The tumor necrosis factor (TNF)-induced necroptosis pathway has been most intensively studied. Upon TNF stimulation when caspase-8 is inhibited or absent [7,8], RIPK1 in complex II recruits RIPK3, resulting in autophosphorylation and activation of the latter. Caspase-8 and FLIP_L in complex II negatively regulates RIPK1 and RIPK3 by proteolysis [9]. Then, these kinases interact with each other via their RIP homotypic interaction motif (RHIM) domains promoting necrosome formation [10], recruitment and phosphorylation of MLKL [11,12] which in turn oligomerizes [13] and is recruited to negatively charged phosphoinositolphosphates [14], causing loss of plasma membrane integrity [15]. Necroptosis contributes to the pathogenesis of several inflammatory diseases including ischemic reperfusion injury, acute pancreatitis, sepsis, neurodegeneration, and viral infection [16]. Although the contribution of necroptosis in liver disease is still an open question [17], some studies reported that necroptosis is also involved in inflammatory-driven liver diseases. On one hand, RIPK3-deficient mice are protected from ethanol- and acetaminophen (APAP)-induced hepatocyte injury or nonalcoholic steatohepatitis (NASH) [18–20]. On the other hand, RIPK3 expression is increased in liver biopsies of chronic ethanol-fed mice, alcoholic liver disease patients, NASH patients, or patients with other chronic liver diseases (hepatitis B and C) [18,20,21]. Furthermore, Nec-1 or Nec-1s protects against APAP- or concanavalin A-induced hepatotoxicity [22–25]. To date, the only possible candidate to be used in the clinic would be the anticancer drug B-RafV600E Dabrafenib which besides mutant Raf targeting also inhibits RIPK3 and alleviates APAP-induced liver injury [26]. Altogether these data suggest that targeting

necroptosis could be a novel therapeutic strategy for liver diseases.

Nec-1 (5-((1H-indol-3-yl)methyl)-3-methyl-2-thioxoimidazolidin-4-one) was identified in a phenotype screen for small molecule inhibiting TNF-induced necroptosis in human monocytic U937 cells [4,27], and further was shown to be an allosteric inhibitor of RIPK1 kinase [6]. However, Nec-1 is not specific for RIPK1 because its chemical scaffold is similar to methyl-thiohydantoin-tryptophan, an inhibitor of indoleamine 2,3-dioxygenase (IDO), an immune regulator [28]. Structure–activity relationship (SAR) study revealed that small substituent Cl at the position 7 of the indole ring leads to the compound necrostatin-1s (Nec-1s) [27] having an increased selective RIPK1 inhibitory activity [29] and lacking IDO inhibitory activity [28]. However, necrostatins have poor pharmacokinetic properties. More recently, other classes of compounds were described such as the 1-aminoisoquinolines, 5-phenylpyrrolo[2,3-b]pyridines, 5-arylpyrrolo[2,3-b]pyridines, furo[2,3-d]pyrimidines, analogs of Bcr-Abl inhibitor ponatinib, PN10 (fusion of the scaffold of ponatinib and Nec-1s), the benzo[b]1,4oxazepin-4-ones, the compound GSK'963, and the *N*-benzyl-*N*-hydroxy-2,2-dimethylbutanamide [30–36]. The previously described biological activities validate kinase RIPK1 as a promising therapeutic target for discovering new compounds to treat various human disorders [37]. The quest for an optimized clinical candidate is still in progress with the synthesis of the first-in-class RIP1 kinase-specific inhibitor (GSK2982772) [38] and will benefit from the description of new potent RIPK1 inhibitors.

In order to find new inhibitors of RIPK1, we screened an in-house kinase-focused library of small chemical compounds (the ReCC, Roscoff essential Chemical Collection, Roscoff, France) using a phenotypic screen based on the inhibition of TNF-induced necroptosis in human FADD-deficient Jurkat T cells (*in vitro* model described in Ref. [39]). Among 1015 tested compounds, 4-(1H-pyrrolo[2,3-b]pyridin-2-yl)phenol [Sibiriline (Sib)] was selected as the best hit. Interestingly, we describe here the biochemical properties and both *in vitro* and *in vivo* effects of this new pyrrolo[2,3-b]pyridine-based derivative as a potent RIPK1 inhibitor/necroptosis inhibitor. Our results indicate that the kinase activity of RIPK1 is dose-dependently affected by Sib. *In silico* molecular modeling and docking studies reveal that Sib interacts with RIPK1 kinase domain in a hydrophobic 'back' pocket [32], between the gatekeeper and the DFG (DLG in RIPK1) motif, adjacent to the adenosine triphosphate (ATP)-binding site, thus locking RIPK1 in an inactive

DLG out conformation. Finally, to assess the therapeutic efficacy of Sib in liver diseases, we studied its effects in concanavalin A-induced hepatitis in C57Bl/6 mice. This acute hepatitis is a mouse model of immune-mediated liver injury [40]. A single intraperitoneal injection of Sib protects mice from liver injury induced by concanavalin A, and therefore, reveals Sib as a promising new chemical scaffold of RIPK1 inhibitor, with a straightforward, high-yielding synthesis, which is effective in the treatment of the preclinical model of immune-dependent hepatitis.

Results

Sibiriline is a new necroptosis inhibitor

To identify novel necroptosis inhibitors, we screened a noncommercial, kinase-focused chemical library of 1015 compounds for their ability to block TNF-induced necroptosis in FADD-deficient human Jurkat cells (Fig. 1A). These compounds were tested at the concentration of 10 μM and compared to the well-characterized RIPK1 inhibitor necrostatin-1 (Nec-1). Among the tested drugs, Sib stood out as the most potent molecule at rescuing cells from necroptotic cell death, whereas Sib-i came out as its inactive analog (Fig. 1B). Similar to Nec-1 ($\text{EC}_{50} = 0.3 \mu\text{M}$), Sib efficiently blocked necroptotic death in FADD-deficient Jurkat cells in a concentration-dependent manner with an EC_{50} value of 1.2 μM (Fig. 1C). The inactive derivative Sib-i was unable to block necroptosis in FADD-deficient Jurkat cells even at the high concentration of 50 μM (Fig. 1C). Importantly, Sib has a very low cytotoxic effect against human peripheral blood leukocytes (PBL) (Fig. 2A) or human retinal pigment epithelial cells (RPE-1 hTERT) (Fig. 2B).

Sib blocks necroptotic but not apoptotic cell death

To further analyze Sib inhibitory effect, we compared the ability of Sib and Nec-1 to block necroptosis in murine and human cell lines *in vitro*. Necroptosis was induced by a wide range of well-described necroptotic stimuli such as TRAIL + zVAD-fmk, TNF + zVAD-fmk, or FasL + zVAD-fmk in human U937 or mouse L929 sAhFas cells. In all of these models, Sib efficiently blocked necroptosis in a dose-dependent manner, and with an efficacy almost similar to Nec-1 (Fig. 3A). This efficient protection from necroptosis by Sib was evidenced by measurements of both plasma membrane permeabilization (% of propidium iodide (PI)-positive cells) and intracellular ATP levels

(Fig. 3A). This latter assay highlighted the fact that Sib inhibitory effect appeared at 2.5 μM and was almost complete at 5 μM . Notably and like Nec-1, Sib did not rescue from apoptosis induced by TRAIL, FasL, or staurosporine in Jurkat cells (Fig. 3B,C), showing that Sib is a selective inhibitor of necroptosis but not of apoptosis. It is to be noted that in a different human cell line resistant to extrinsic apoptosis, the FADD-deficient Jurkat cells, TNF-induced necroptosis can also be prevented by Sib. Conversely, Fas-induced apoptosis in the L929 sAhFas mouse model is not sensitive to Sib (data not shown). Overall, these data evidenced that Sib specificity toward inhibiting necroptosis, but not apoptosis, does not depend upon the stimuli, the cell type, or even the species.

Sib rescues cells from necroptosis even after cell death initiation and allows cell survival and proliferation

In the hypothetical perspective of using Sib as a necroptosis inhibitor in medicine, we tested its activity when administered after, rather than before, necroptosis initiation. In the following experimental setup, Sib or Nec-1 was added at the nontoxic concentration of 10 μM between 1 to 4 h after TNF-dependent necroptosis induction in FADD-deficient Jurkat cells. When added in the first couple of hours following necroptosis induction, Sib promotes an almost complete recovery by decreasing cell death to approximately 10%. When added 3 or 4 h after necroptosis induction, both Sib or Nec-1 treatment rescued necroptotic FADD-deficient Jurkat cells, reducing by a minimum of 50% the number of PI-positive cells (Fig. 4A). To further refine Sib's potential at preventing cells from a necroptotic wave, a clonogenic assay was performed 24 h after necroptosis induction by TNF + zVAD-fmk in L929 cells in the presence or absence of Sib, Sib-i, Nec-1, or Nec-1s. Eight days later, culture plates were stained with crystal violet and showed that treatment with Sib, Nec-1, or Nec-1s but not with Sib-i allowed the formation of colonies (Fig. 4B), suggesting that Sib as other well-known necroptosis inhibitors (Nec-1 or Nec-1s), not only protected cells from cell death but also allowed them to survive and proliferate.

Sib is a potent inhibitor of RIPK1

In order to investigate the mechanism of action of Sib and its target, the selectivity of Sib and Sib-i was tested at 10 μM against a panel of 456 kinases including eight lipid kinases in an *in vitro* competition binding assay (KINOMEscan; DiscoverX, San Diego, CA,

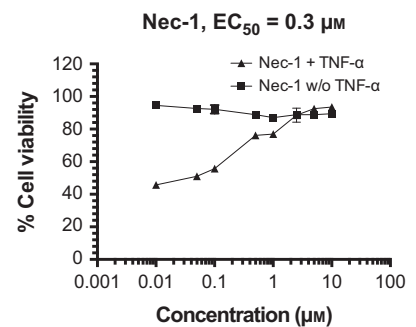
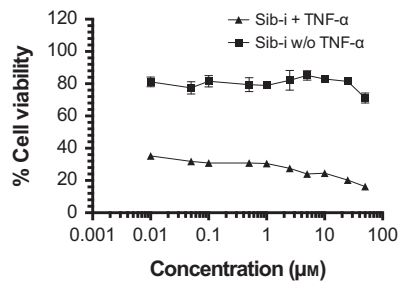
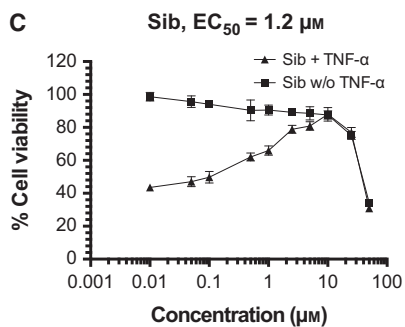
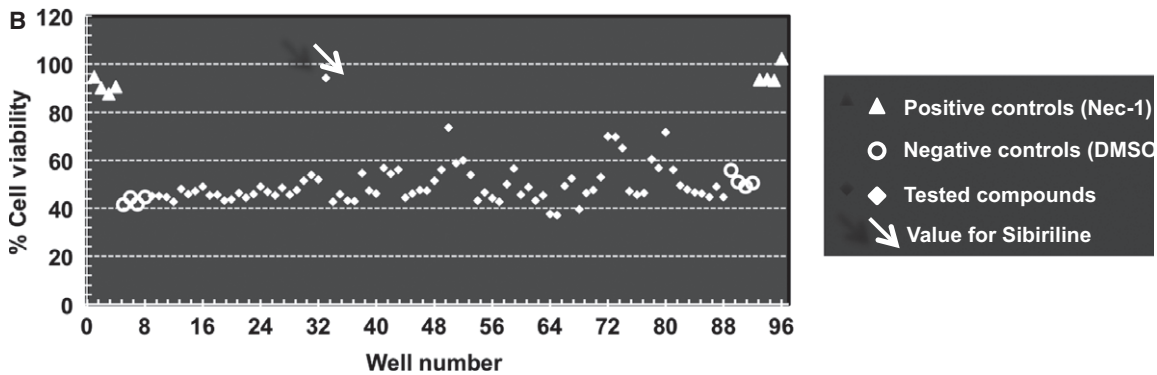
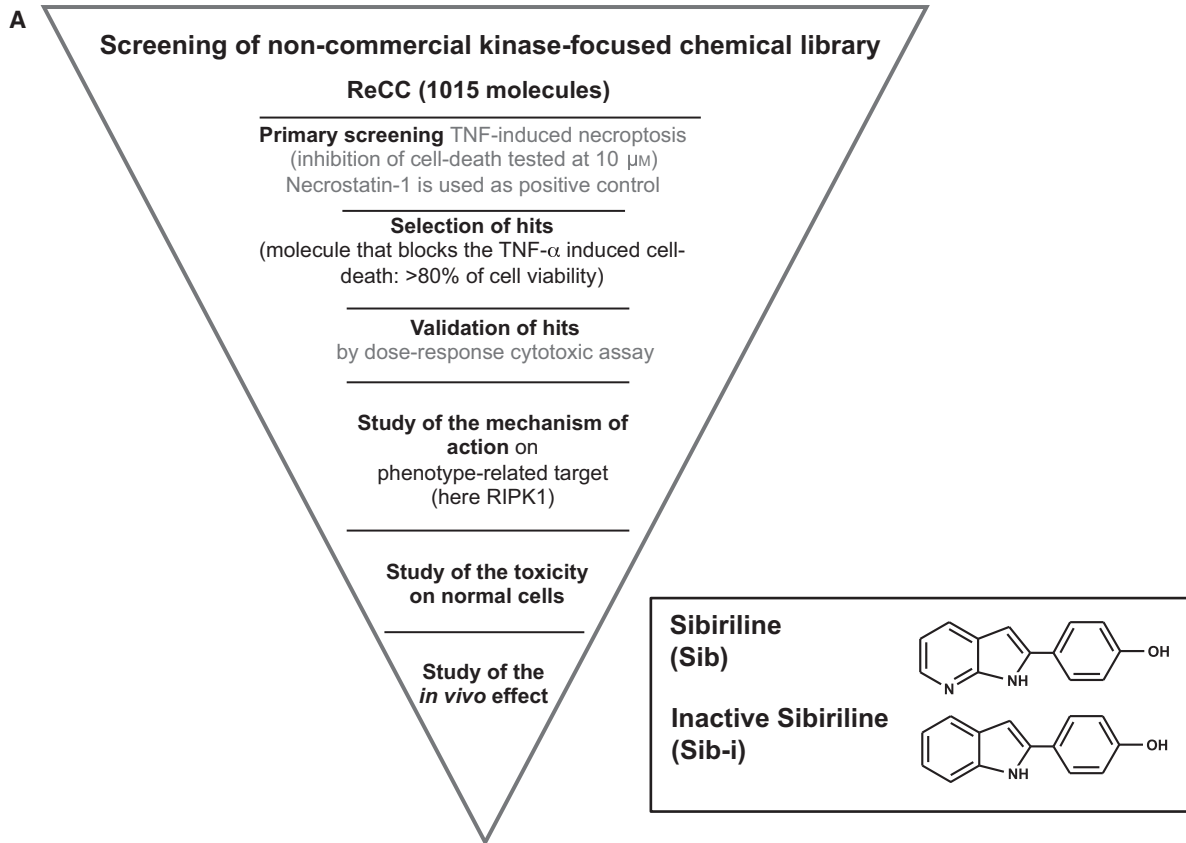


Fig. 1. Identification of Sibiriline as potent necroptosis inhibitor by cell-based screening of chemical library. (A) Workflow of the cell-based selection of new necroptosis inhibitors. Among 1015 compounds, 4-(1H-pyrrolo[2,3-b]pyridin-2-yl)phenol (Sibiriline, Sib) was selected as an inhibitor of TNF α -induced necroptosis in human FADD-deficient Jurkat cells. The different steps of the selection are reported in the inverted triangle. Inactive Sibiriline (Sib-i) was not detected during the screening campaign and is thus considered as the negative control of Sibiriline. (B) Results of the automated cell-based screening assay highlighting putative necroptosis inhibitor candidates shown in scatter plot. Ninety-six compounds were screened per plate (including eight positive and eight negative controls) for their antinecrototic activity on Jurkat FADD-deficient cell line treated with TNF- α . Cell viability was evaluated by 3-(4,5-dimethylthiazol-2-yl)-5-(3-carboxymethoxyphenyl)-2-(4-sulfophenyl)-2H-tetrazolium (MTS) reduction assay, 24 h after addition of tested compounds on cells and is expressed in % of survival in cells treated with DMSO. The primary screening is performed in monoplicate. (C) Dose-dependent inhibition of TNF- α -induced necroptosis by increasing concentrations of Sibiriline. After a 24-h incubation, the effect of the tested compound on the cell viability was evaluated by MTS reduction assay and is expressed in % of survival in cells treated with DMSO ($n = 3$, mean \pm SD).

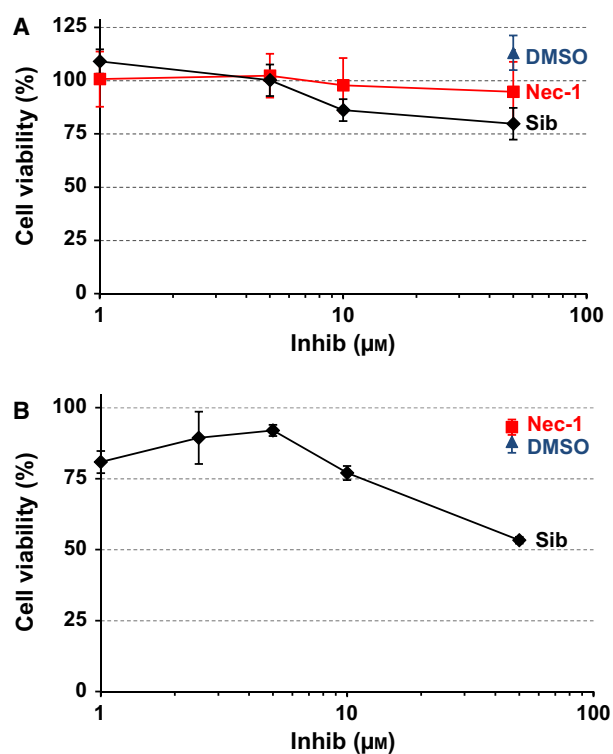


Fig. 2. At inhibitory concentration, Sibiriline is not toxic toward human primary leukocytes or retina cells. Twenty-four hour after Sibiriline treatment, cell viability was measured with an MTS assay to determine the toxicity of the compound toward either (A) human primary blood leukocytes (hPBLs, $n = 6$ individuals, mean \pm SD) or (B) human retina pigmented epithelium cells (RPE-1 hTERT, $n = 3$, mean \pm SD).

USA). RIPK1 was shown to be among the top kinases targeted by Sib as only 0.2% of the initial amount of the kinase was still on the affinity matrix after competition with Sib (Table S1 and blue circle on Fig. 5A). Sib-i is not a potent interactor of the tested kinases (Fig. 5A). Death-associated protein kinase-3 (DAPK3) is only poorly affected by Sib-i (32% of the initial amount of kinase is still on the affinity matrix after competition with 10 μ M Sib-i, Fig. 5A). Using this

competition binding assay, the dissociation constant (K_d) of Sib for RIPK1 was calculated with a standard dose-response curve and showed the high affinity of Sib for RIPK1 with a K_d in nM range and equal to 218 nM (Fig. 5B, left panel). High affinity of Nec-1 or Nec-1s for RIPK1 was also confirmed with K_d equal to 31 nM or 8 nM, respectively (Fig. 5B, right panel).

To further confirm the inhibition of RIPK1 enzymatic activity by Sib, an *in vitro* autophosphorylation assay using recombinant full-length RIPK1 (GST-tagged) was performed. This assay showed an inhibition of RIPK1 autophosphorylation by Sib in a dose-dependent manner, Sib-i having no effect (Fig. 6A). The catalytic activity of RIPK1 was also quantified by monitoring the phosphorylation of myelin basic protein (MBP), a known substrate of RIPK1. Consistently, Sib efficiently inhibits the phosphorylation of MBP in a dose-dependent manner with an IC_{50} equal to 1.03 μ M (Fig. 6B).

Finally, to characterize the mechanism of RIPK1 inhibition by Sib, we analyzed the effect of increasing the concentrations of ATP (up to 1 mM of cold ATP) on the inhibition of autophosphorylation by 10 μ M of Sib. Results obtained show that in the presence of 1 mM cold ATP, the inhibition of the RIPK1 autophosphorylation by Sib was decreased. It suggests an ATP-competitive mechanism of RIPK1 inhibition by Sib (Fig. 6C). This result was previously described for Nec-1 [6]. Very interestingly, Sib had a very low inhibitory effect on RIPK3 kinase activity with an IC_{50} equal to 101.9 μ M (Fig. 6D). Altogether, these data demonstrated that Sib is a specific inhibitor of RIPK1 kinase activity. In agreement with this biochemical activity, Sib was able, with a similar efficacy to Nec-1, to inhibit RIPK1-dependent necroptosis induced by the combination TNF + TAK1i + zVAD-fmk by reducing the percentage of Syber Green (% SG)-positive cells measured in function of time (Fig. 7A, left panel). This necroptotic pathway was characterized by the lack of caspase-3 activity (very low DEVD-AMC fluorescence) (Fig. 7A, right panel).

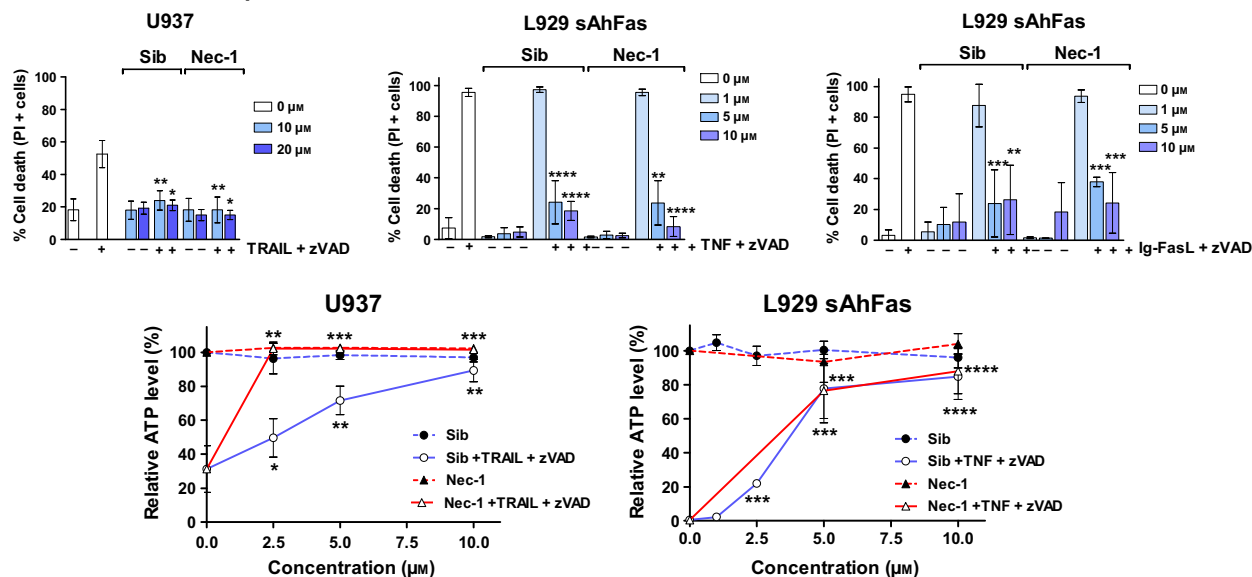
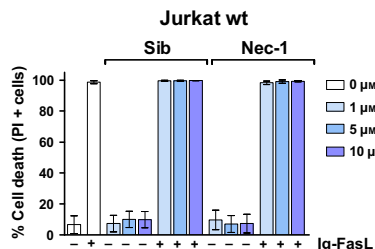
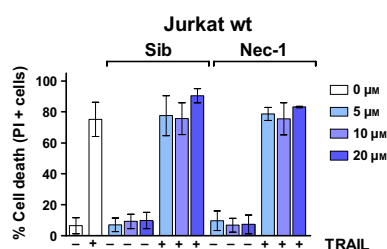
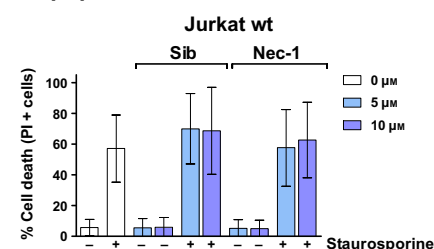
A DR-induced necroptosis**B DR-induced apoptosis****C DR-independent induced apoptosis**

Fig. 3. Sibiriline inhibits death receptor-induced necroptosis but not apoptosis. (A) Necroptosis was induced in U937 cells by a pretreatment with zVAD-fmk (20 µM) followed by a 24-h treatment with TRAIL-Flag (10 ng·mL⁻¹). In L929 sAhFas cell line, the same zVAD-fmk pretreatment was followed either with a TNF (10 ng·mL⁻¹) or an Ig-FasL (200 ng·mL⁻¹) 16-h treatment. The percentage of cell death was determined by propidium iodide staining using flow cytometry (upper panels) ($n = 3$, mean \pm SEM, * $P < 0.05$, ** $P < 0.01$, *** $P < 0.001$ and **** $P < 0.0001$). Intracellular ATP levels (lower panels) were measured with the CellTiter-Glo[®] Luminescent Cell Viability Assay ($n = 3$, mean \pm SEM, * $P < 0.05$, ** $P < 0.01$, *** $P < 0.001$ and **** $P < 0.0001$). Apoptosis was induced in Jurkat wild-type cells with either (B) a TRAIL-Flag (10 ng·mL⁻¹) or Ig-FasL (200 ng·mL⁻¹) or (C) staurosporine (100 nM) 18-h treatment. The percentage of cell death was quantified by flow cytometry using propidium iodide staining ($n = 3$, mean \pm SD). Results shown are representative of at least three independent experiments.

Moreover, Sib like Nec-1 inhibited RIPK1-dependent apoptosis induced by the combination of TNF + TAK1i [41,42] by decreasing both the % SG-positive cells and caspase-3 activity measured as a function of time (Fig. 7B).

Molecular modeling of the RIPK1–Sib complex

To further understand the mechanism of inhibition by the small chemical compound, we studied *in silico* the RIPK1–Sib complex to establish a possible model of RIPK1 inhibition by Sib. Molecular docking simulations of Sib to RIPK1 kinase and molecular dynamics

trajectory computed for the best complex indicated a preferential binding mode similar to the one described for Nec-1s on a site next to the ATP-binding site (Figs 8 and 9). Contact residues determined included notably the seven key amino acids (Leu70, Val76, Leu78, Leu90, Asp156, Ser161, and Phe162) (Fig. 8A) involved in the interaction with necrostatins (see [43] for details on RIPK1–Necrostatins complexes). An exhaustive list of surrounding residues (3.5 Å cut-off) also included the amino acids Met67, Lys77, Lys79, Met92, Val134, and Ile154 (Fig. 9). Note here that Met92 is the gatekeeper residue of RIPK1 [6] and the catalytic triad residues are Lys45, Glu63, and Asp156

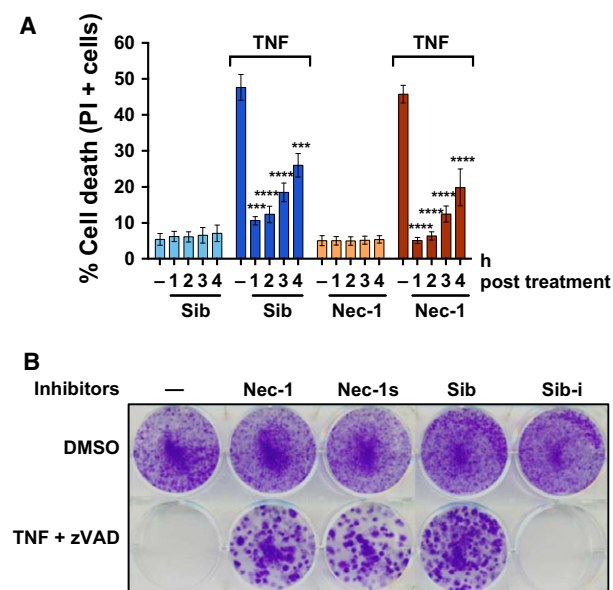


Fig. 4. Sibiriline remains effective at preventing necroptosis when applied post cell death initiation and allows cell survival and proliferation. (A) Viability was assessed by flow cytometry with propidium iodide (PI) staining on FADD-deficient Jurkat cells treated with TNF ($10 \text{ ng}\cdot\text{mL}^{-1}$) followed by $10 \mu\text{M}$ Sibiriline (Sib) or necrostatin-1 (Nec-1) addition 1–4 h post necroptosis initiation ($n = 4$, mean \pm SEM, *** $P < 0.001$ and **** $P < 0.0001$). (B) Clonogenic assay was performed in L929 cells. Twenty-four hour after TNF+zVAD-fmk treatment in the absence or presence of $10 \mu\text{M}$ necroptosis inhibitors (Nec-1, Nec-1s, or Sib) or $10 \mu\text{M}$ Sib-i, 1000 cells per well were plated and stained with crystal violet 8 days later. One representative of three experiments is shown.

as reported [43]. Sib thus binds in the ‘back’ pocket of RIPK1 between the DLG motif and the gatekeeper. Despite the presence of a canonical H-bond donor/H-bond acceptor motif, Sib, like Nec-1s, does not appear to bind to the hinge region, at least in this conformation of the protein (Fig. 8B,C).

In contrast, the inactive compound Sib-i did not contact the C-lobe region of RIPK1 (Fig. 9). Comparison between the contact residues predicted for active compounds (Sib and Nec-1s) and inactive compound (Sib-i) did indicate the position of a good inhibitor that should promote hydrophobic interactions with the long helix defined by residues from Pro111 to Lys132, thus locking the conformation of the enzyme by reducing the mobility of the two main subdomains of the kinase toward each other (Fig. 9).

Sib protects mice from concanavalin A-induced hepatitis

The identification of Sib as a specific necroptosis and RIPK1 inhibitor as Nec-1 prompted us to test this

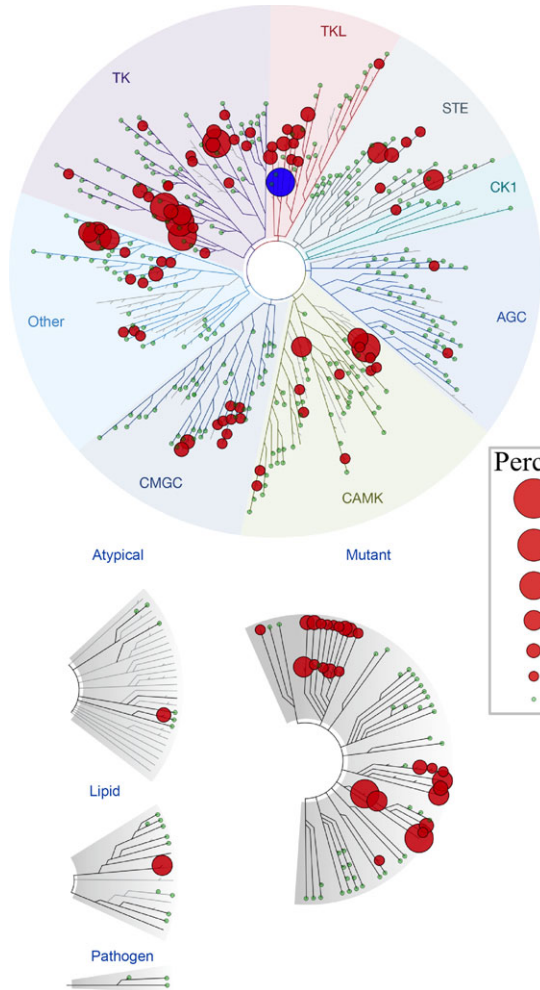
compound in a murine model of immune-dependent hepatitis induced by concanavalin A treatment. In this model, we have previously demonstrated a protective effect of an intravenous injection of Nec-1 or Nec-1s against concanavalin A-induced hepatitis [22,25]. Here, we studied the protective effect of an intraperitoneal injection of $3 \text{ mg}\cdot\text{kg}^{-1}$ Sib or $6.25 \text{ mg}\cdot\text{kg}^{-1}$ Nec-1s 1 h before an intravenous injection of $12 \text{ mg}\cdot\text{kg}^{-1}$ concanavalin A.

Pretreatment with either Sib or Nec-1s protected mice from concanavalin A-induced hepatotoxicity by significantly decreasing serum aspartate aminotransferase (AST)/alanine aminotransferase (ALT) levels measured 24 h after treatment (Fig. 10A). Moreover, Sib or Nec-1s significantly decreased liver damage by reducing the size of perivascular and parenchymal zones of necrosis stained with hematoxylin and eosin (Fig. 10B, see arrows) and the percentage of necrotic area (Fig. 10C). In accord with the protection afforded by Sib or Nec-1s, the loss of mouse body weight induced by concanavalin A treatment was significantly reduced by Sib or Nec-1s pretreatment (Fig. 11). Altogether these data suggest that $3 \text{ mg}\cdot\text{kg}^{-1}$ Sib had an almost comparable efficacy to $6.25 \text{ mg}\cdot\text{kg}^{-1}$ Nec-1s in protecting mice against concanavalin A-induced hepatitis.

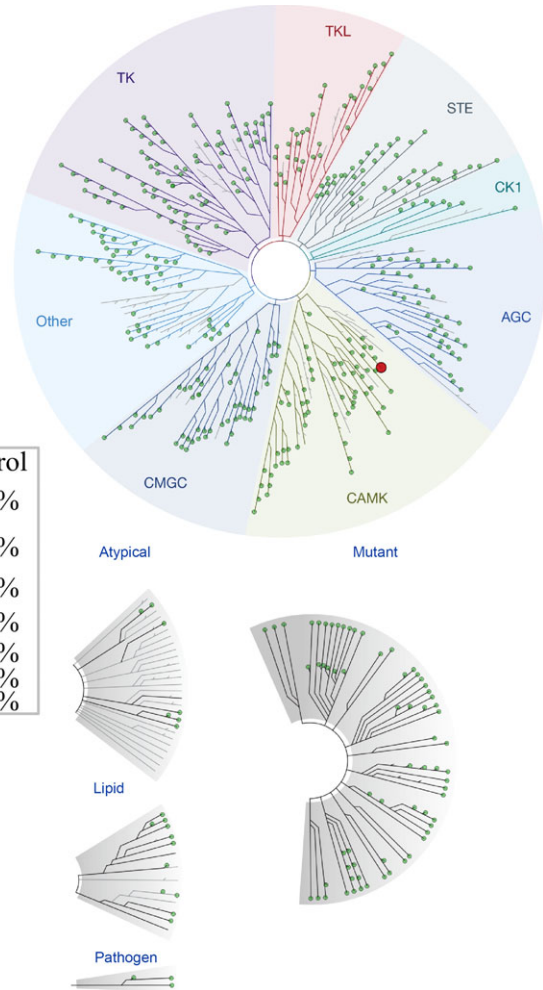
Discussion

By using a cellular screen and a unique noncommercial, kinase-focused chemical library of 1015 small molecular compounds, we identified a new inhibitor of TNF-induced necroptosis in Jurkat FADD-deficient cells with a micromolar EC_{50} concentration. Sib, 4-(1H-pyrrolo[2,3-b]pyridin-2-yl)phenol is a new pyrrolo[2,3-b]pyridine-based derivative compound. Our present data enlarge the number of small chemical compounds having a potent necroptosis inhibitory activity [44]. Sib was also able to inhibit TRAIL- or FasL-induced necroptosis but not apoptosis regardless of the human or murine cell line origin. Protection from necroptotic cell death was obtained at 1–5 μM concentration of Sib in our diverse cellular systems, suggesting a large therapeutic window for potential clinical application. Moreover, protection from necroptosis has been afforded by Sib up to 4 h after the induction of death, which could allow a therapeutic potential in the case of cardiac infarction or stroke. Regarding the mode of action underlying necroptosis inhibition by Sib, a KINOMEScan competition binding assay at DiscoverX (456 kinases and activated mutant kinases) was performed and showed that RIPK1 was the top kinase inhibited by Sib. In

A **Sib** (456 assays tested)
104 interactions mapped
S-Score(35) = 0.197



Sib-i (456 assays tested)
1 interaction mapped
S-Score(35) = 0.003



B

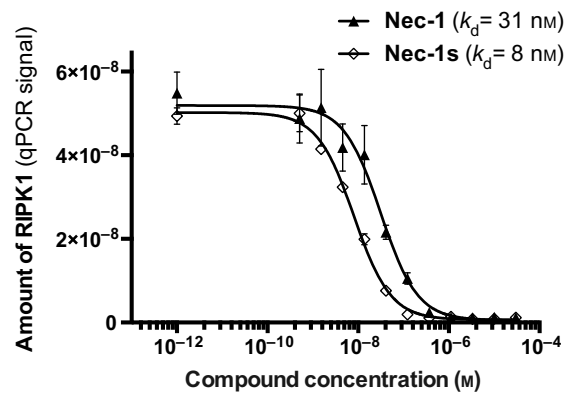
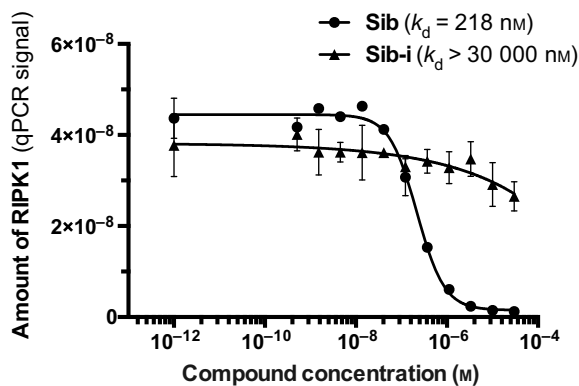
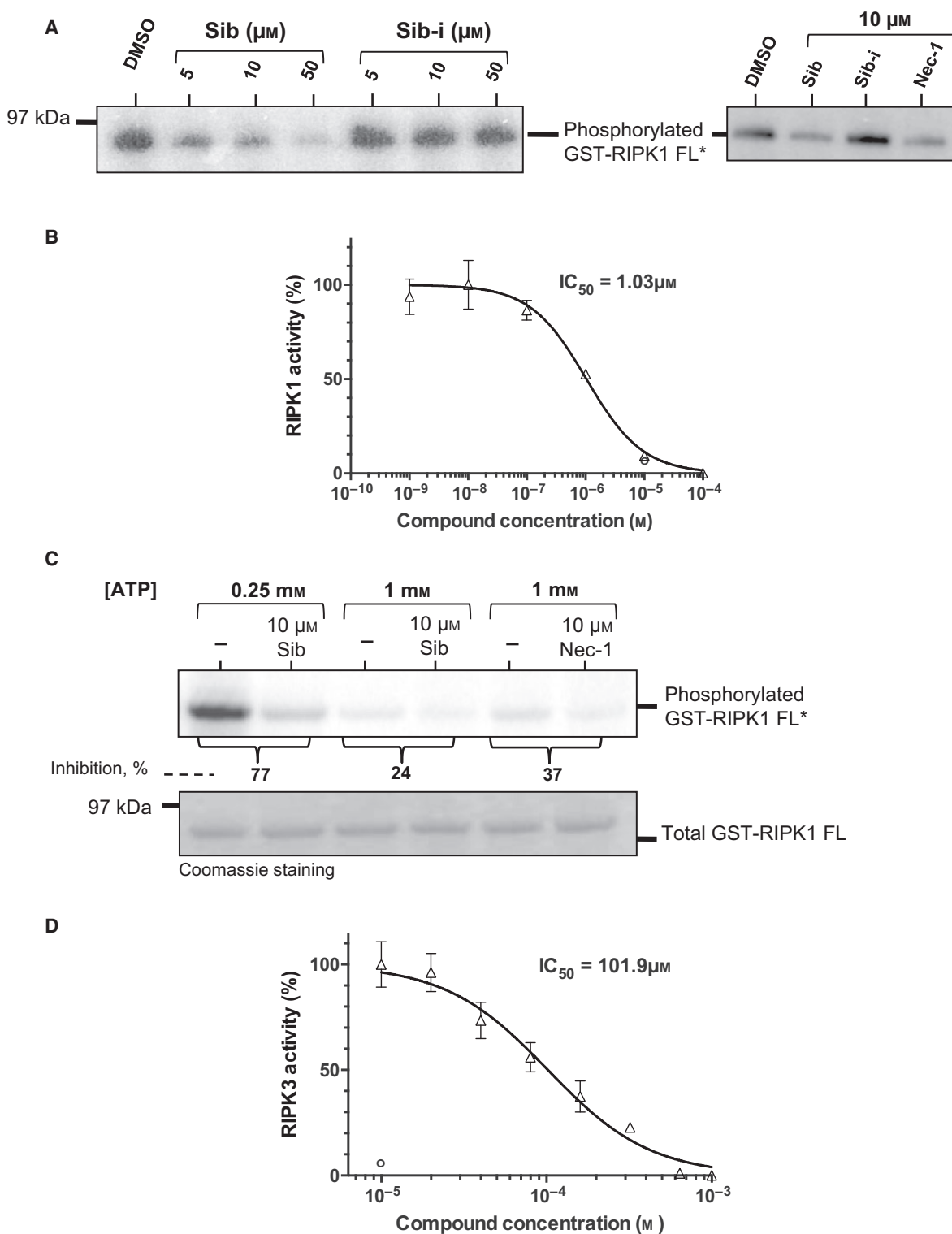


Fig. 5. Study of the binding of Sibiriline to RIPK1 and to a large panel of kinases. (A) Biochemical kinase profiling assay (KINOMEScanSM) which measures drug binding with a panel of 456 purified kinases (mostly human). This TREEspotTM Kinase dendrogram (DiscoverX) is an artistic representation of the human kinome phylogenetic tree. The codes reported on this figure indicate the subclasses of protein kinases: CMGC for CDKs, MAP kinases, GSK and CDK-like kinases; AGC for protein kinase A, G, and C families (PKA, PKC, PKG); CAMK for Ca²⁺/calmodulin-dependent protein kinases; CK1, cell kinases 1 (originally known as casein kinase 1); STE, STE kinases (homologs of yeast STERile kinases); TKL, tyrosine kinases-like; TK, tyrosine kinases. Each kinase tested in the assay panel is marked with a circle. The hit kinases reported are marked with a red circle, except RIPK1 which is marked with a blue circle. 0% represents the higher affinity, whereas small green dots indicate that at the tested concentration of molecule (here 10 μ M), Sib or Sib-i cannot bind significantly to the kinase (as over 35% of the tested kinase are still on the affinity matrix after competition with the tested compound). For RIPK1, only 0.2% of the initial amount of kinase is still on the affinity matrix after competition with 10 μ M Sibiriline (the full list of results for Sibiriline is reported in Table S1). Selectivity Score (reported on the figure as S-Score) is a value related to compound selectivity. It is calculated by dividing the number of kinases that compounds bind to by the total number of distinct kinases tested, excluding mutant variants. S-Score(35) = (number of nonmutant kinases with %Ctrl < 35)/(number of nonmutant kinases tested). Images were generated using TREEspotTM Software Tool and reprinted with permission from KINOMEScan[®], a division of DiscoverX Corporation. (B) Measure of the binding constant for RIPK1/Sibiriline interaction. An 11-point threefold serial dilution of Sib, Sib-i, Nec-1, or Nec-1s were prepared in 100% DMSO in order to determine the binding constant (K_d). K_d s are calculated by measuring the amount of kinase captured on the solid support as a function of the test compound concentration ($n = 2$, mean \pm SEM).

contrast to Nec-1 which did not bind to RIPK2 and RIPK4 [45], Sib bound to RIPK4 to a certain extent (Table S1). We showed in this study that the kinase activity of RIPK3 is only poorly affected by Sib (approximately 100 times less potently inhibited compared to RIPK1). The KINOMEScan also revealed that JAK2, PDGFR β , KIT, and KIT (V559D) are other major kinases targeted by Sib. Chemical synthesis of Sib analogs, notably driven by the molecular docking reported in this study, would be necessary to improve the selectivity of this compound. As expected, no kinase was efficiently targeted by the inactive counterpart, Sib-i. We also determined a K_d binding constant of Sib for RIPK1 of 218 nM, whereas the K_d of Sib-i was greater than 30 000 nM. The *in vitro* competitive assay used for both K_d study and kinase profiling is based on an active site/ligand binding technology developed by DiscoverX (Fremont, CA, USA): it can detect the effect of compounds that bind the kinase active site and directly (sterically) or indirectly (allosterically) prevent kinase binding to one immobilized ligand. The majority of kinase inhibitors developed to date target the ATP-binding site. Based on the selectivity reported for Sib, we hypothesized that Sib also targets the ATP-binding site of RIPK1. We showed here that ATP competes with Sib for the inhibition of RIPK1 autophosphorylation (Fig. 6C). Such result was already described for Nec-1 [6], suggesting some similarities in the mode of action between Sib and Nec-1. *In silico* molecular modeling and docking studies highlighted these similarities. To understand the interaction mode of Sib with RIPK1, molecular docking was performed based on the cocrystal structure of RIPK1 with Nec-1s (PDB: code 4ITH). The predictive binding mode was shown on Fig. 8. As was the case for Nec-1s, Sib was located in the hydrophobic ‘back’

[32] pocket between the N-lobe and C-lobe of the RIPK1 kinase domain, interacting with both the DLG motif and the gatekeeper. This pocket is formed by a number of residues including Leu70, Val76, Leu78, Leu90, Asp156, Ser161, and Phe162 (see [43] for details on RIPK1-Necrostatins complexes). In analogy with the inhibition of RIPK1 by Nec-1s, we hypothesized that Sib locks RIPK1 in an inactive conformation (‘DLG (Asp-Leu-Gly)-out’ state of kinase) notably by interaction with Asp156 of the DLG motif and neighboring Ser161. Interactions with the C-lobe also appear to be an important element for successful inhibition. Our results suggest that Sib shares characteristics of the type II kinase inhibitor class, which target the inactive enzymatic conformation, with the caveat that it does not interact with the hinge region, despite its H-bond donor–H-bond acceptor motif. As the description of the druggability of necroptosis [4], numerous chemobiological studies have led to the discovery of molecules that can bind to the catalytic site of RIPK1 [37]. As examples, compounds characterized by a GlaxoSmithKline group include notably pyrrolo [2,3 b]pyridine-based derivatives [30]. Interestingly, and similar to the putative mechanism of Sib described here, these small chemical compounds also share all characteristics of the type II kinase inhibitor class. This class of compounds is believed to perturb the Phe side chains of the catalytic site inwards to obstruct the ATP-binding cleft.

As Nec-1 or Nec-1s has already been shown to protect mice from concanavalin A-induced hepatitis [22,24,25], we tested the effect of Sib in this model of murine hepatitis. Pretreatment of mice with 3 mg·kg⁻¹ Sib has almost the same protective effect against concanavalin A-induced hepatitis than pretreatment of mice with 6.25 mg·kg⁻¹ Nec-1s, by decreasing serum



AST/ALT levels and liver injury. Sib seems to have no toxic adverse effect as this compound allowed mice to recover some weight after concanavalin A treatment.

Altogether these data demonstrated efficacy of Sib *in vivo* which make Sib to be a highly promising template for lead optimization.

Fig. 6. Effect of Sibiriline on the catalytic activity of RIPK1. (A) RIPK1 was treated with 5, 10, or 50 μM of the mentioned chemical compound to analyze the effect on the kinase autophosphorylation. Radioactive autophosphorylation assays were processed with ATP- γ - ^{32}P at 30 μM final concentration. Necrostatin-1, a well-described inhibitor of RIPK1, was used as an internal control. Coomassie staining was performed in order to estimate the total amount of protein loaded on polyacrylamide gel. Autophosphorylated RIPK1 band was visualized on radiographic film. Assays were performed at least two times, and similar results were obtained each time. The representative images are shown: (B) Sibiriline inhibits the catalytic activity of RIPK1. GST-RIPK1 full length produced by baculovirus in Sf9 insect cells was assayed in the presence of increasing concentrations of Sibiriline with myelin basic protein, MBP, as a substrate. Kinase activities are expressed in % of maximal activity, i.e., measured in the absence of inhibitor. The value marked with a circle corresponds to 10 μM Nec-1s ($n = 3$, mean \pm SD). (C) High concentration of ATP has an effect on the inhibition of RIPK1 autophosphorylation by Sibiriline. The cold ATP (0.25 or 1 mM) was used to study the competition with Sibiriline. These assays are similar to those described in (A). Necrostatin-1, a known ATP-competitive inhibitor of RIPK1, was used as an internal control. % of RIPK1 activity inhibition is calculated through a ratio with DMSO (-), as a 0 percent reference. The normalization between samples was performed using the quantification of proteins. (D) No effect of Sibiriline on the catalytic activity of RIPK3. GST-RIPK3 full length produced by baculovirus in Sf9 insect cells was assayed in the presence of increasing concentrations of Sibiriline with myelin basic protein, MBP, as a substrate. Kinase activities are expressed in % of maximal activity, i.e., measured in the absence of inhibitor. The value marked with a circle corresponds to 10 μM of GSK'872, a reference RIPK3 inhibitor ($n = 3$, mean \pm SD).

Materials and methods

Cell lines and culture conditions

SV40 large T-immortalized mouse embryonic fibroblasts (MEFs) and L929 sAhFas were kind gifts of the University of Ghent (Belgium). These cell lines were cultured in

Dulbecco's modified Eagle's medium (DMEM) high glucose (Invitrogen/Thermo Fisher Scientific, Villebon sur Yvette, France) supplemented with 10% FCS and 2 mM L-glutamine (Invitrogen/Thermo Fisher Scientific). HT29, Jurkat wild-type A3, FADD-deficient Jurkat I 2.1, L929, U937, RPE-1 hTERT human cell lines were obtained from ATCC (American Type Culture Collection, Rockville, MD,

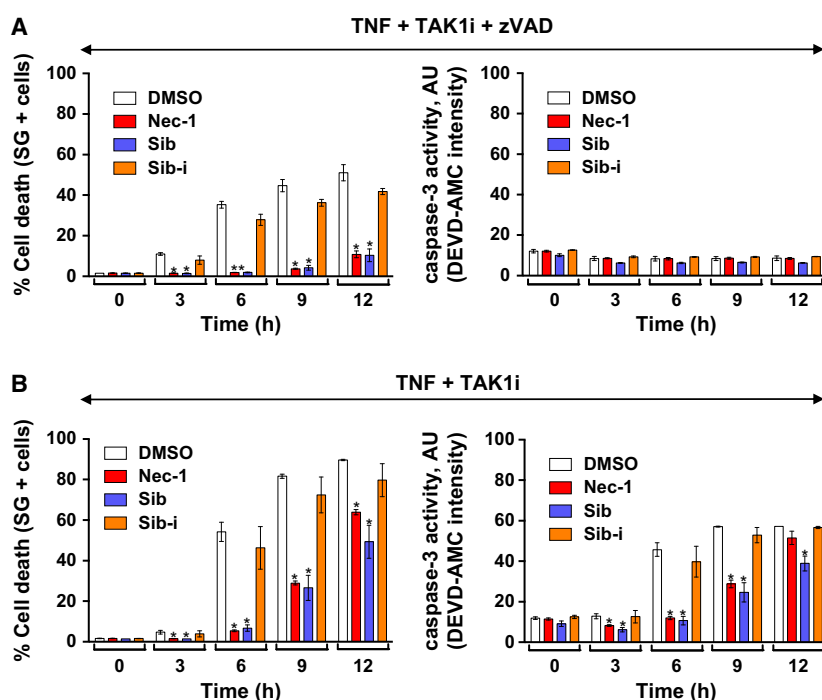


Fig. 7. Sibiriline prevents RIPK1-dependent cell death upon TNF stimulation. The percentage of cell death (SytoxGreen fluorescence intensity) and caspase-3 activity expressed in arbitrary units (DEVD-AMC fluorescence intensity) were measured in function of the time by using a Fluostar Omega fluorescence plate reader as described in Materials and methods. MEF cells were pretreated or not (DMSO) with the indicated compounds (Nec-1, Sib, Sib-i) at 10 μM and TAK1i at 1 μM \pm zVAD-fmk at 20 μM for 1 h and then treated with hTNF (600 IU·mL $^{-1}$). (A) Effect of Sibiriline on RIPK1-dependent necroptosis induced by TNF+TAK1i+zVAD in immortalized MEFs (% cell death, $n = 3$, mean \pm SD, $*P < 0.05$; caspase-3 activity AU, $n = 3$, mean \pm SD, $*P < 0.05$). Results shown are representative of at least three independent experiments. (B) Effect of Sibiriline on RIPK1-dependent apoptosis induced by TNF+TAK1i in immortalized MEFs. (% cell death, $n = 3$, mean \pm SD, $*P < 0.05$; caspase-3 activity AU, $n = 3$, mean \pm SD, $*P < 0.05$). Results shown are representative of at least three independent experiments.

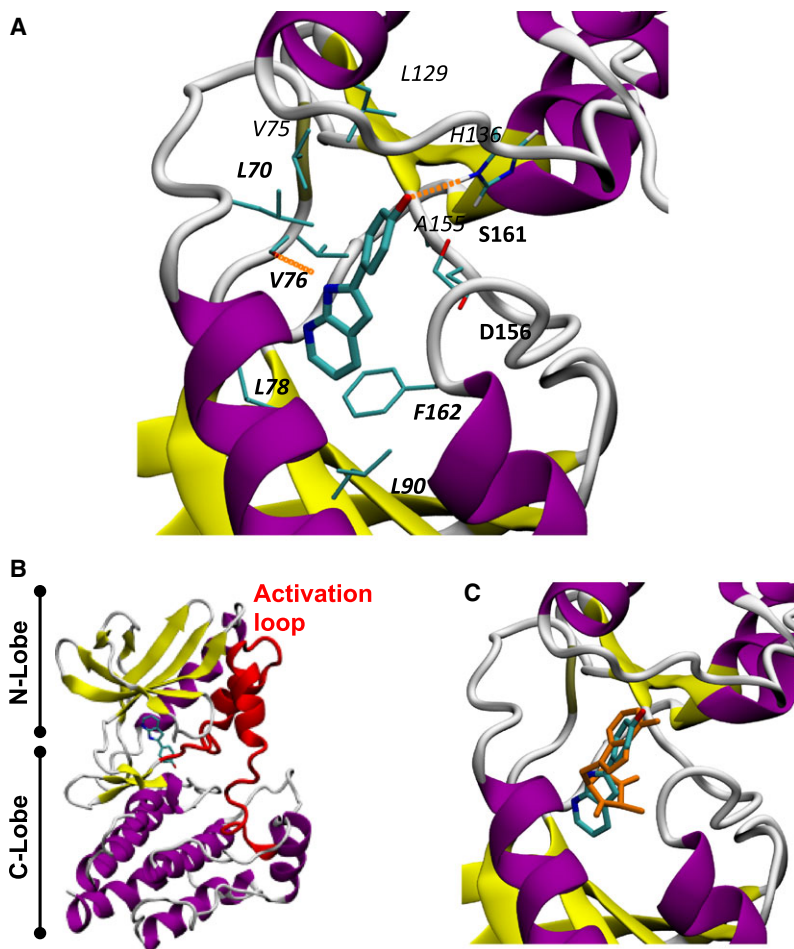


Fig. 8. Sibiriline interacts closely to the RIPK1 ATP-binding pocket. (A) Close-up view of the interaction between Sib and surrounding residues in RIPK1 reporting the contact residues determined after MD optimization of the best position of Sib obtained upon docking: (a) Bold residues are the seven key amino acids involved in the interaction with necrostatins (as reported in Xie *et al.*) [40]; (b) italic residues are defining the pharmacophore derived from LigandScout analysis. (B) View of the overall structure of Sib-bound RIPK1 highlighting the bridging contact performed by Sib between both protein subdomains. Activation loop defined by residues Asp156 to Glu196 is shown in red. (C) Superimposition of the model to the X-ray structure 4ITH obtained for the complex formed by Nec-1s (orange sticks) with RIPK1.

USA). HT29 cells were cultured in EMEM (Eurobio, Les Ulis, France) supplemented with 10% FCS and 2 mM L-glutamine. Jurkat, FADD-deficient Jurkat and U937 cells were cultured in RPMI containing Glutamax (Invitrogen/Thermo Fisher Scientific) supplemented with 15% FCS. RPE-1 hTERT cells were cultured in DMEM-F12 containing Glutamax (Invitrogen/Thermo Fisher Scientific) supplemented with 10% FCS. All cells were cultured under a 5% CO₂ atmosphere at 37 °C.

Chemicals and biological compounds

Recombinant human Flag-tagged TRAIL (TRAIL-Flag) and zVAD-fmk were obtained from Enzo Life Sciences (Villeurbanne, France). Necrostatin-1 (Nec-1) and necrostatin-1s (Nec-1s) were from Calbiochem (VWR International, Fontenay-sous-Bois, France). The TAK1 kinase inhibitor, NP-009245, was from AnalytiCon Discovery GmbH (Postdam, Germany). Anti-Flag M2 IgG1 antibody, cycloheximide (CHX), and PI were obtained from Sigma-Aldrich (St Quentin-Fallavier, France). TNF α were obtained from Invitrogen/Thermo Fisher Scientific. This TNF α was used in the screen of new necroptosis inhibitors. Recombinant human TNF α was

also produced and purified to at least 99% homogeneity at VIB Protein service facility (Ghent, Belgium). It has a specific biological activity of 6.8×10^7 IU·mg⁻¹ and was used at 2000 IU·mL⁻¹ (67 ng·mL⁻¹) in FADD-deficient Jurkat or at 600 IU·mL⁻¹ (20 ng·mL⁻¹) in MEFs. The multiaggregated Ig-CD95L (or Ig-FasL) was a kind gift of Dr P. Legembre (CLCC Eugene Marquis, Rennes, FR) and was used at 200 ng·mL⁻¹.

Synthesis of 4-(1H-pyrrolo[2,3-b]pyridin-2-yl)phenol (Sib): following literature procedure [46], a solution of 3-picoline (200 mg, 2.2 mmol, 1 eq) in anhydrous THF (10 mL) was added dropwise to a solution of LDA (freshly prepared by adding nBuLi (1.5 mL, 2.5 M solution in hexanes, 3.9 mmol) to diisopropylamine (0.54 mL, 3.9 mmol) in anhydrous THF (10 mL)) at 0 °C under argon atmosphere. The orange mixture was stirred for 20 min before dropwise addition of a solution of 4-methoxybenzotrile (316 mg, 2.2 mmol, 1 eq) in anhydrous THF (10 mL). After 1 h at 0 °C, more LDA solution in THF (10 mL, 3.9 mmol, prepared as above) was added dropwise and the reaction was slowly warmed to RT over 1 h before being heated to reflux in a water bath for 2 h. After cooling, the yellow solution was quenched carefully with saturated

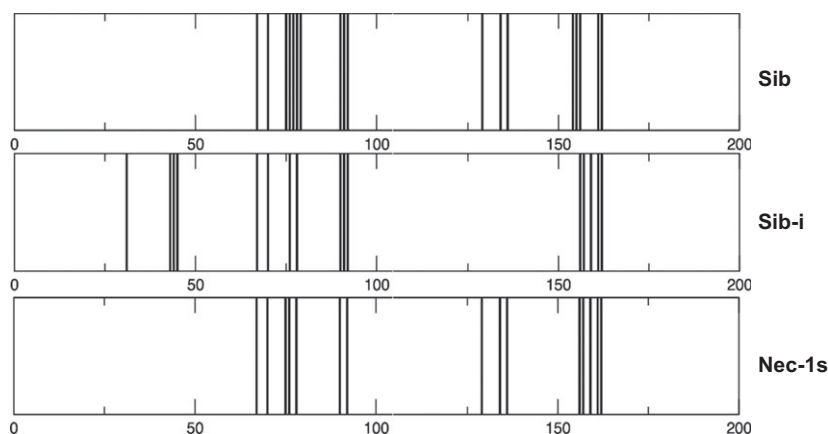


Fig. 9. Contact residues (3.5 Å cut-off distance) predicted for the interaction of active and inactive inhibitors with human RIPK1, in comparison with those of the experimental Nec-1s-RIPK1 structure. Comparison between active compounds (Sib, top row and Nec-1s, bottom row) and the inactive compound (Sib-i, middle row) indicates that the inactive compound shares many of the interactions with one or both active inhibitors, with the notable exception of the contacts with the residues between 129 and 136, which are present in both active inhibitors. The position of a good inhibitor should therefore promote hydrophobic interactions with the end of the long C-domain helix defined by residues 111Pro to 132Lys, thereby reducing the mobility of the two main subdomains of the kinase toward each other.

NH₄Cl (10 mL) and water (40 mL) was added. The precipitate was filtered, washed with diethyl ether and water, dried under vacuum to afford 2-(4-methoxyphenyl)-1H-pyrrolo[2,3-b]pyridine as a light yellow solid (327 mg, 68%). Analytical data are in accordance with the literature.

2-(4-methoxyphenyl)-1H-pyrrolo[2,3-b]pyridine (100 mg, 0.44 mmol) was suspended in anhydrous dichloromethane (5 mL) and cooled to -78°C . Boron tribromide (1.3 mL of 1 M solution on dichloromethane, 1.3 mmol, 3 eq) was added dropwise and the dark red mixture was stirred for 16 h while warming to RT. The reaction was carefully quenched with water, dichloromethane (10 mL) was added, and the solid was dissolved by addition of 1 M sodium hydroxide (15 mL). After stirring for 10 min, the aqueous phase was washed with dichloromethane (2×10 mL) and the pH was adjusted to 5 with 1 M hydrochloric acid. The resulting precipitate was filtered, washed with water, and dried under vacuum to obtain a tan solid (68 mg, 74%). ¹H NMR (300 MHz, DMSO-d₆): 11.93 (bs, 1H), 9.71 (bs, 1H), 8.14 (dd, $J = 4.7, 1.3$ Hz, 1H), 7.85 (dd, $J = 7.8, 1.3$ Hz, 1H), 7.76 (d, $J = 8.7$ Hz, 2H), 7.02 (dd, $J = 7.8, 4.7$ Hz, 1H), 6.85 (d, $J = 8.7$ Hz, 2H), 6.70 (d, $J = 2.0$ Hz, 1H). ¹³C NMR (75 MHz, DMSO-d₆): 157.7, 149.6, 141.9, 139.0, 127.1, 126.9, 122.7, 121.3, 115.9, 115.8, 95.1. MS (ESI): m/z 211 [M+H]⁺. Synthesis of the inactive derivative Sib-i has been described previously [47].

Cell-based screening assay for characterization of necroptosis inhibitors

The details of the cell-based assay used to screen a library of small chemical compounds have been described in Miao and Degterev [39]. The Jurkat FADD-deficient I 2.1 cell line was maintained in RPMI 1640 medium (Gibco/Thermo Fisher

Scientific, Carlsbad, CA, USA) containing Glutamax and 15% fetal calf serum (Eurobio). Necroptosis was induced by addition of $10\text{ ng}\cdot\text{mL}^{-1}$ of human recombinant TNF- α (Invitrogen/Thermo Fisher Scientific). Necrostatin-1 (Nec-1; Calbiochem) was used as model necroptosis inhibitor. Cells were maintained in 75 cm² flask and passaged every 2 or 3 days. Chemical collections analyzed were formatted in 96-well plates with 80 molecules per plate at 10 mM in 100% DMSO. For each collection plate, two cell plates were seeded (one treated with TNF- α and the other one without TNF- α). Cells were seeded at 20 000 cells per well, in 40 μL of medium, in a 96-well clear, flat bottom plate (CytoOne, Starlab) before treatment. Then, 40 μL of medium with or without TNF- α at $25\text{ ng}\cdot\text{mL}^{-1}$ was added to all wells in the corresponding plate. Immediately after TNF- α addition, 20 μL of diluted compound at 50 μM was added to the plates. Final concentration of each chemical compound was 10 μM at 0.1% DMSO. Eight positive (Nec-1 at 10 μM final) and eight negative (DMSO) controls were used in each plate to validate the assay. Cells were incubated at 37°C , 5% CO₂ for 24 h before performing MTS viability assay, described hereafter. Compounds were diluted before treating cells. Liquid handling was performed using the Nimbus Microlab liquid handler (Hamilton Robotics, Bonaduz, Switzerland) under microbiological safety workbench. The stock solutions of compounds at 10 mM were diluted directly in culture medium to obtain a solution at 50 μM before treating cells.

Cell death assays

Cell viability was measured by a water soluble tetrazolium compound MTS (3-[4,5-dimethylthiazol-2-yl]-5-[3-carboxymethoxyphenyl]-2-[4-sulfophenyl]-2H-tetrazolium, inner salt) (CellTiter 96[®] AQueous Non-Radioactive Cell Proliferation

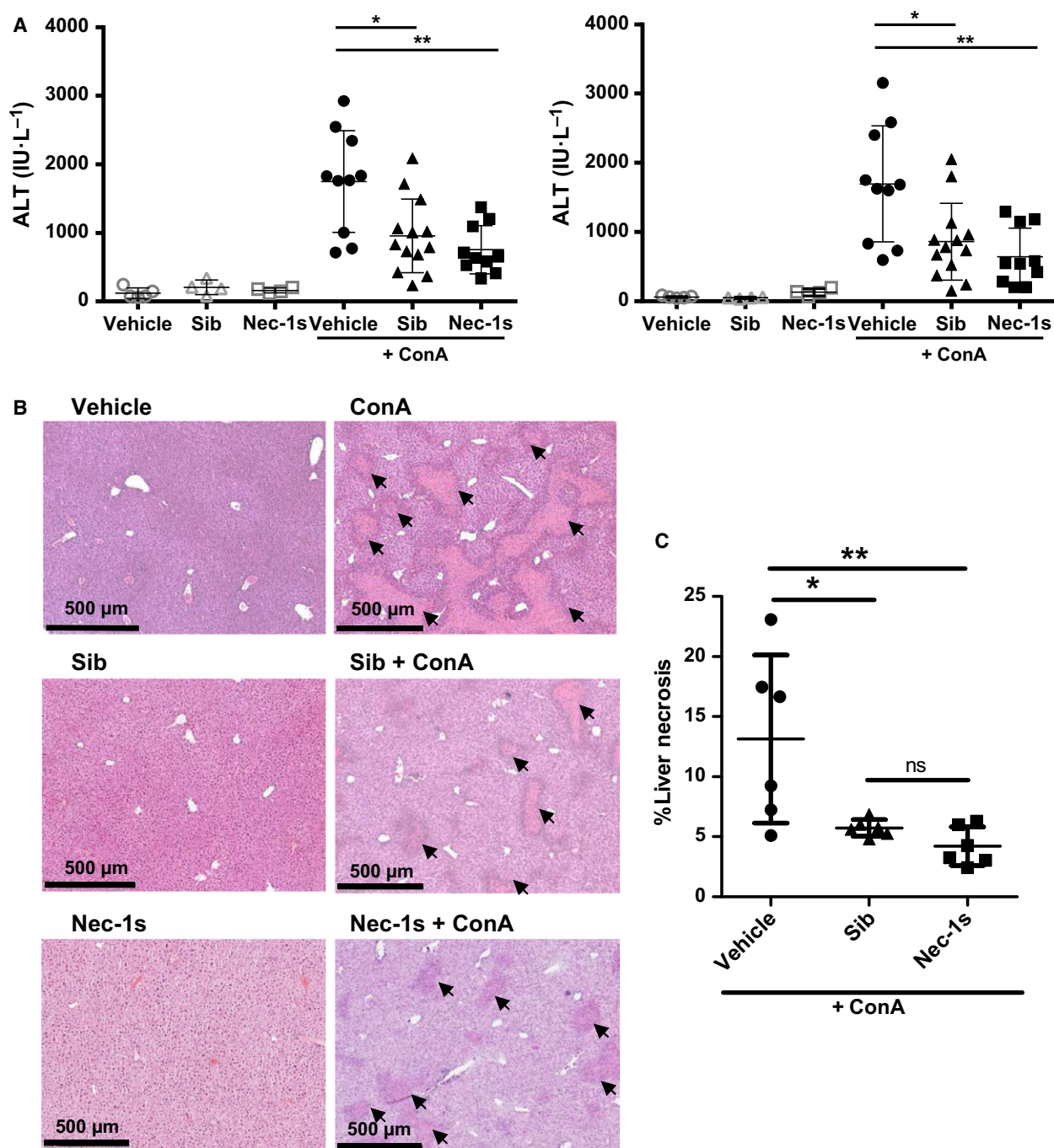


Fig. 10. Sibiriline prevents concanavalin A-induced hepatitis *in vivo*. C57Bl/6 WT mice were pretreated for 1 h with intraperitoneal administration of 3 mg·kg⁻¹ Sib or 6.25 mg·kg⁻¹ Nec-1s diluted in vehicle before intravenous administration of 12 mg·kg⁻¹ concanavalin A. At the end of treatment, mice were sacrificed (vehicle, $n = 5$; Sib, $n = 4$; Nec-1s, $n = 4$; vehicle + concanavalin A, $n = 10$; Sib + concanavalin A, $n = 13$; Nec-1s + concanavalin A, $n = 10$). (A) Serum levels of AST and ALT were determined at 24 h post-concanavalin A injection as described in Materials and methods. Mean \pm SEM * $P < 0.05$ and ** $P < 0.01$. (B) Hematoxylin and eosin-stained liver sections were shown. Scale bars represent 500 μ m. (one picture representative for each group of mice). (C) Percentage of liver necrosis was determined 24 h after concanavalin A treatment in each group (vehicle + concanavalin A, $n = 6$; Sib + concanavalin A, $n = 6$; Sib + concanavalin A, $n = 6$) as described in Materials and methods. Mean \pm SEM * $P < 0.05$ and ** $P < 0.01$.

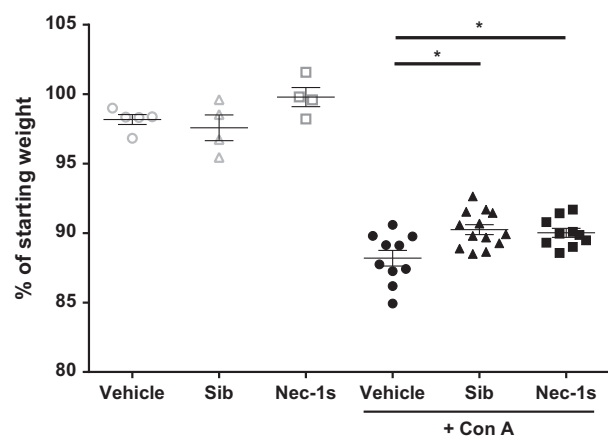


Fig. 11. Sibiriline reduces the loss of mouse body weight induced by concanavalin A treatment. C57Bl/6 WT mouse body weights were determined 24 h post-treatment in each group (vehicle, $n = 5$; Sib, $n = 4$; Nec-1s, $n = 4$; vehicle + concanavalin A, $n = 10$; Sib + concanavalin A, $n = 13$; Nec-1s + concanavalin A, $n = 10$). Mean \pm SEM * $P < 0.05$.

Assay; Promega, Fitchburg, WI, USA), according to the manufacturer's instructions. This method is based on the reduction of MTS tetrazolium compound by viable cells to generate a colored formazan product. Human peripheral blood leukocytes (PBL) and human RPE-1 hTERT cells were seeded in 96-well plates at 2.5×10^5 or 8×10^3 cells per well, respectively. After 24 h of treatment, 20 μ L of assay solution was added. After 3-h incubation at 37 $^{\circ}$ C, the absorbance at 490 and 630 nm was measured by a microplate reader (SPECTROstar Nano, BMG Labtech). The results were corrected by subtracting the background reading (after 2-h incubation with blank medium) and viability was calculated with % viability = mean (OD₄₉₀ - OD₆₃₀) sample / mean (OD₄₉₀ - OD₆₃₀) control \times 100.

Detection of necrotic cells was done by using PI staining (500 ng·mL⁻¹) and flow cytometry analysis. U937, Jurkat, or L929 sAhFas cell lines were seeded at 2.5×10^5 cells per well in 24-well plates. Concerning necroptotic models, U937 cells were pretreated with zVAD-fmk (30 μ M) for 30 min and then treated for 20 h with TRAIL-Flag (200 ng·mL⁻¹) and 2 μ g·mL⁻¹ M2 anti-Flag antibody. L929 sAhFas cells were pretreated with zVAD-fmk (20 μ M) for 30 min and then with TNF (10 ng·mL⁻¹) or Ig-FasL (200 ng·mL⁻¹) for 16 h. FADD-deficient Jurkat cells were treated with 10 ng·mL⁻¹ TNF. As for apoptotic models, wild-type Jurkat cells were treated either with TRAIL-Flag (20 ng·mL⁻¹) and 2 μ g·mL⁻¹ M2 anti-Flag antibody, Ig-FasL (200 ng·mL⁻¹), or staurosporine (100 nM) for 18 h. After treatment, percentage of PI-positive cells was determined by flow cytometry analysis of fluorescence (FL-2) (FACScalibur, Becton Dickinson, Le Pont de Claix, France) and expressed as %/NT.

Clonogenic assay

After treatment with TNF/zVAD-fmk in the presence or absence of inhibitory compounds (Sib, Sib-i, Nec-1, or Nec-1s) as described above, L929 cells were seeded out in an appropriate dilution, here 1000 cells per well (in six-well plates), and allow for 8 days to form colonies. The subsequent colonies were fixed with ice cold methanol and stained with crystal violet (50% ethanol).

RIPK1 and RIPK3 kinase assays

Human RIPK1 full-length GST-tagged was expressed by baculovirus in Sf9 insect cells (product #R07-10G; SignalChem, Richmond, CA, USA). The protocol used to detect the enzymatic activity is adapted from Degterev *et al.* [6]. For detection of RIPK1 autophosphorylation, kinase reaction was initiated mixing 5 μ L of RIPK1, 5 μ L of 3 \times kinase reaction buffer (5 mM MOPS pH 7.2, 2.5 mM glycerol 2-phosphate, 4 mM MgCl₂, 2.5 mM MnCl₂, 1 mM EGTA, 0.4 mM EDTA, 50 μ g·mL⁻¹ BSA, or 0.05 mM DTT), 2 μ L H₂O, and 3 μ L of the tested molecule. The mixture was kept on ice for 10 min. During the incubation, the ATP solution was prepared by mixing 5 μ L of 3 \times kinase reaction buffer, 4 μ L H₂O, 6 μ L cold ATP at 150 μ M, and 2 μ Ci of [γ -³²P] ATP. This ATP solution was then mixed with RIPK1 and the tested compound, and was incubated for 30 min at 30 $^{\circ}$ C. Reactions were stopped by boiling in 5 μ L of loading buffer for 3 min at 95 $^{\circ}$ C. Twenty-five microliter of each reaction were loaded per well in precast NuPage 12% Bis-Tris gel (Thermo Fisher Scientific) and analyzed by SDS/PAGE. Autophosphorylated RIPK1 band was visualized by analysis in a Typhoon Phosphorimager (GE Healthcare Life Sciences, Velizy-Villacoublay, France). Alternatively, the kinase activity of RIPK1 can be detected using the 'gold standard' P81 phosphocellulose assay. Note here that the P81 ion exchange chromatography paper (GE Healthcare) used in this study is no longer provided by the manufacturer. For a final volume of 30 μ L, 2 μ L of kinase was assayed in buffer described above with 0.1 μ g· μ L⁻¹ of MBP (#M1891; Sigma) as substrate and in the presence of 15 μ M [γ -³³P] ATP (3000 Ci·mmol⁻¹; 10 mCi·mL⁻¹). Controls (maximal kinase activity) were performed with appropriate dilutions of dimethylsulfoxide. After extensive washes with a solution of phosphoric acid at 1% in water using a FilterMate Harvester (PerkinElmer, Waltham, MA, USA), the wet filters were counted in the presence of 20 μ L ACS (GE Healthcare) scintillation fluid using a TopCount[®] Scintillation and Luminescence Counter (PerkinElmer).

The kinase activity of RIPK3 (human, recombinant, expressed by baculovirus in Sf9 insect cells) was detected in RIPK1 buffer with 0.1 μ g· μ L⁻¹ of MBP as substrate following the P81 phosphocellulose assay described here before.

Kinase binding assays

Binding assays were performed by DiscoverX (Fremont). These assays are based on a competition binding assay that quantitatively measures the ability of a compound to compete with an immobilized, active site-directed ligand. See Fabian *et al.* for details on this assay technology [48]. In brief, streptavidin-coated magnetic beads were mixed with biotinylated small-molecule ligands to generate affinity resins for the assay. After blocking, binding reactions were assembled by combining DNA-tagged kinases, inhibitors, and liganded affinity beads. The ability of the tested compound to compete with the immobilized ligand is measured via quantitative PCR of the DNA tag. The percent inhibition was calculated by measuring the amount of kinase captured on the solid support as a function of the test compound concentration. In this study, binding assays were used for (a) the analysis of selectivity against a large panel of kinases (service 'KINOMEScan') and for (b) the determination of binding constant (K_d) of small chemical compound for RIPK1 (service 'KdELECT'). Dissociation constants (K_d s) are calculated by measuring the amount of kinase captured on the solid support as a function of the test compound concentration with top concentration being 30 000 nM.

Analysis of cell death and caspase-3 activation

Mouse embryonic fibroblasts were seeded at 7500 cells per well in 96-well plates. The next day, cells were pretreated with the indicated compounds for 30 min and then stimulated with human TNF ($600 \text{ IU}\cdot\text{mL}^{-1}$) in combination with $1 \mu\text{M}$ TAK1i with or without $20 \mu\text{M}$ zVAD-fmk in the presence of $5 \mu\text{M}$ SytoxGreen (Invitrogen/Thermo Fisher Scientific) and $20 \mu\text{M}$ DEVD-MCA (PeptaNova GmbH, Sandhausen, Germany). SytoxGreen intensity and caspase-3 activation were measured at intervals of 1 h using a Fluostar Omega fluorescence plate reader (BMG Labtech GmbH, Ortenberg, Germany), with excitation/emission filters of 485/520 nm for SytoxGreen and 360/460 nm for DEVD-MCA, gains set at 1100, 20 flashes per well, and orbital averaging with a diameter of 3 mm. Percentage of cell death was calculated as $(\text{induced fluorescence} - \text{background fluorescence}) / (\text{maximal fluorescence} - \text{background fluorescence}) \times 100$. The maximal fluorescence is obtained by full permeabilization of the cells using Triton X-100 at a final concentration of 0.1%. The caspase-3 activity was calculated as $(\text{induced DEVD-AMC fluorescence} - \text{background fluorescence}) \times 100 / (\text{SytoxGreen fluorescence obtained from the Triton X-100 permeabilized cells})$.

ATP concentration measurement

U937 and L929 sAhFas were seeded at 2×10^4 cells per well in white 96-well plates for 24 h. U937 cells were pretreated with zVAD-fmk ($30 \mu\text{M}$) for 30 min and then

treated for 20 h with TRAIL-Flag ($200 \text{ ng}\cdot\text{mL}^{-1}$) and $2 \mu\text{g}\cdot\text{mL}^{-1}$ M2 anti-Flag antibody. L929 sAhFas cell line were pretreated with zVAD-fmk ($20 \mu\text{M}$) for 30 min and then treated with mouse TNF ($10 \text{ ng}\cdot\text{mL}^{-1}$) or Ig-FasL ($200 \text{ ng}\cdot\text{mL}^{-1}$) for 16 h. Concentration of cellular ATP was measured using CellTiter-Glo[®] Luminescent Cell viability assay (Promega) according to the manufacturer's instruction and as previously described [22]. ATP concentration was expressed as $\%/\text{NT} \pm \text{SD}$.

Molecular docking

In order to complete the RIPK1 structure available from PDB structures, we performed homology modeling of full RIPK1 protein, notably for the completion of the missing residues. The selected template was ITHJ_B as only loop ¹⁷⁷REVDGTAKKNGG¹⁸⁸ was missing in this structure. Homology modeling did not seem reliable because it did not propose any structuration of this loop despite PSSPred results predicting that a majority of residues should be involved in alpha-helix secondary structure. PEPFold ab-initio method allowed us to model the loop efficiently and finally enabled us to complete the RIPK1 model for molecular docking computations. Next, a normal mode analysis (NMA) was achieved with EInemo program to modulate the RIPK1 conformations available from the initial model, improving the variety of protein structures that will be used during docking by the addition of two more models for RIPK1 after modes selection (following EInemo standard validation of essential modes). The final three models of RIPK1 were used as biological target (receptor) for the exploration of possible association modes with compounds Nec-1s, Sib, and Sib-i. Docking calculations were performed by using the standard protocol proposed in the VINA implementation of YASARA suite (global docking, 1000 runs per target/per compound). Results have been clusterized, thanks to the g cluster command of the Gromacs program (Jarvis-Patrick method). After ranking of the poses, the best positioning of the ligand toward the receptor (energy criteria) was submitted to a short molecular dynamics simulation in water for 10 ns in order to improve the model of compound-RIPK1 complex. Final models were obtained after energy minimization after checking that the ligand was stable during the MD trajectory. Ligand-contacting residues were detected using a 3.5 \AA cut-off distance and pharmacophores were derived from a standard analysis by using Ligand Scout program.

Concanavalin A-induced hepatitis

Seven- to nine-week-old female C57Bl/6 WT mice were purchased from Janvier (Le Genest St Isle, France). Concanavalin A was provided by Sigma-Aldrich and diluted at $12 \text{ mg}\cdot\text{kg}^{-1}$ in PBS/5% DMSO (vehicle). C57Bl/6 WT mice were pretreated for 1 h with intraperitoneal administration

of 3 mg·kg⁻¹ Sib or 6.25 mg·kg⁻¹ Nec-1s diluted in vehicle before retro-orbital administration of 12 mg·kg⁻¹ concanavalin A for 24 h. At the end of treatment, mice were sacrificed (vehicle, *n* = 5; Sib, *n* = 4; Nec-1s, *n* = 4; vehicle + concanavalin A, *n* = 10; Sib + concanavalin A, *n* = 13; Nec-1s + concanavalin A, *n* = 10). All animals received human care and all study protocols comply with the institution's guidelines. Authors were authorized to lead animal experimentation by 'La direction des Services Vétérinaires' (license M Samson #A3523840), and the project was authorized by the Comité Régional d'Ethique d'Expérimentation Animal CREA (license given by the 'Ministère de l'Education Nationale et de la Recherche' # 7576).

At the end of the experiment, mice body weights were measured and fragments of mouse livers were fixed in 4% paraformaldehyde and embedded in paraffin for hematoxylin/eosin staining. Serum AST and ALT were measured in mouse serum according to the IFCC primary reference procedures and using the Olympus AU2700 Autoanalyser (Olympus France, Rungis, France). The percentage of liver necrosis was determined using image analysis software (NDP view, Hamamatsu). The total liver area taken into account was comprised between 18 and 51 mm².

Statistical analyses

Data presented were acquired from a minimum of three independent experiments. They are expressed as means ± SD or ± SEM. Statistical analyses for *in vitro* studies were performed with unpaired *t* tests. For *in vivo* studies, Mann-Whitney *U* test was used for comparison of control group parameters with treatment group. All statistical analyses were performed with GRAPHPAD PRISM6 software (GraphPad Software, San Diego, CA, USA).

Acknowledgements

Dr. Sandrine Ruchaud is warmly acknowledged for her continuing support and critical reading of the manuscript. We thank Béatrice Foll-Josselin for cell culture and Mathieu Bertrand and Kathrin Weber for helpful scientific advices. The authors also thank the Cancéropôle Grand-Ouest (axis: Nature sea products in cancer treatment), GIS IBiSA (Infrastructures en Biologie Santé et Agronomie, France), and Biogenouest (Western France life science and environment core facility network) for supporting KISSf screening facility (Roscoff, France). We also thank the animal house facilities and the immunohistology platform (Biosit, Rennes). Michel Samson, Stéphane Bach, and Marie-Thérèse Dimanche-Boitrel were supported by INCA PLBIO2012 ("NECROTRAIL" Program). MT Dimanche-Boitrel's group was also supported by grants from Conseil Régional de Bretagne (ID2 Santé),

and the Ligue Contre le Cancer (committees Ille et Vilaine and Maine et Loire). F Faurez was supported by INCa (postdoctoral fellow). M Bonnet was supported by the European University of Brittany (Chaire d'excellence). Research in the group of Prof. P. Vandenabeele is supported by grants from the Vlaams Instituut voor Biotechnologie (VIB), from Ghent University (MRP, GROUP-ID consortium), grants from the 'Foundation against Cancer' (2012-188 and FAF-F/2016/865), grants from the Fonds voor Wetenschappelijk Onderzoek Vlaanderen (FWO) (FWO G.0875.11, FWO G.0A45.12N, FWO G.0787.13N, FWO G.0C37.14N, FWO G.0E04.16N), grants from the Flemish Government (Methusalem BOF09/01M00709 and BOF16/MET_V/007), a grant from the Belgian science policy office (BELSPO) (IAP 7/32). This work is part of shared PhD ship between universities of Rennes and Ghent.

Author contributions

FLC designed, performed, and analyzed *in vitro* and *in vivo* data. CD designed, performed, and analyzed *in vitro* data and protein kinase production and phosphorylation. SL-P designed, performed, and analyzed *in vitro* data. AF designed, performed, and analyzed *in vivo* data. AC synthesized the compounds and characterized them by RMN and mass spectrometry. OD conducted *in silico* molecular modeling and docking analyses. ND was in charge of cell culture, MTS viability assay, and autophosphorylation assay. BB was in charge of protein kinase purification and phosphorylation assays. IG was in charge of cell culture and MTS assay. CPP designed, performed, and analyzed *in vivo* data. FF designed and performed *in vitro* data. MB designed and performed *in vivo* data. YM was the chemist who synthesized the compound Sib for the first time. PG analyzed results of chemical synthesis and revised the manuscript. MS designed, performed, and analyzed *in vivo* data. PV revised the manuscript. SB and MTDB participated in the study, design, and coordination. All the authors read and approved the final manuscript submitted for publication.

References

- 1 Malhi H, Guicciardi ME & Gores GJ (2010) Hepatocyte death: a clear and present danger. *Physiol Rev* **90**, 1165–1194.
- 2 Saeed WK & Jun DW (2014) Necroptosis: an emerging type of cell death in liver diseases. *World J Gastroenterol* **20**, 12526–12532.

- 3 Zhao H, Jaffer T, Eguchi S, Wang Z, Linkermann A & Ma D (2015) Role of necroptosis in the pathogenesis of solid organ injury. *Cell Death Dis* **6**, e1975.
- 4 Degtarev A, Huang Z, Boyce M, Li Y, Jagtap P, Mizushima N, Cuny GD, Mitchison TJ, Moskowitz MA & Yuan J (2005) Chemical inhibitor of nonapoptotic cell death with therapeutic potential for ischemic brain injury. *Nat Chem Biol* **1**, 112–119.
- 5 Vanden Berghe T, Linkermann A, Jouan-Lanhouet S, Walczak H & Vandenabeele P (2014) Regulated necrosis: the expanding network of non-apoptotic cell death pathways. *Nat Rev Mol Cell Biol* **15**, 135–147.
- 6 Degtarev A, Hitomi J, Gernscheid M, Ch'en IL, Korkina O, Teng X, Abbott D, Cuny GD, Yuan C, Wagner G *et al.* (2008) Identification of RIP1 kinase as a specific cellular target of necrostatins. *Nat Chem Biol* **4**, 313–321.
- 7 Vercammen D, Brouckaert G, Denecker G, Van de Craen M, Declercq W, Fiers W & Vandenabeele P (1998) Dual signaling of the Fas receptor: initiation of both apoptotic and necrotic cell death pathways. *J Exp Med* **188**, 919–930.
- 8 Duprez L, Takahashi N, Van Hauwermeiren F, Vandendriessche B, Goossens V, Vanden Berghe T, Declercq W, Libert C, Cauwels A & Vandenabeele P (2011) RIP kinase-dependent necrosis drives lethal systemic inflammatory response syndrome. *Immunity* **35**, 908–918.
- 9 Oberst A, Dillon CP, Weinlich R, McCormick LL, Fitzgerald P, Pop C, Hakem R, Salvesen GS & Green DR (2011) Catalytic activity of the caspase-8-FLIP(L) complex inhibits RIPK3-dependent necrosis. *Nature* **471**, 363–367.
- 10 Li J, McQuade T, Siemer AB, Napetschnig J, Moriwaki K, Hsiao YS, Damko E, Moquin D, Walz T, McDermott A *et al.* (2012) The RIP1/RIP3 necrosome forms a functional amyloid signaling complex required for programmed necrosis. *Cell* **150**, 339–350.
- 11 Sun L, Wang H, Wang Z, He S, Chen S, Liao D, Wang L, Yan J, Liu W, Lei X *et al.* (2012) Mixed lineage kinase domain-like protein mediates necrosis signaling downstream of RIP3 kinase. *Cell* **148**, 213–227.
- 12 Murphy JM, Czabotar PE, Hildebrand JM, Lucet IS, Zhang JG, Alvarez-Diaz S, Lewis R, Lalaoui N, Metcalf D, Webb AI *et al.* (2013) The pseudokinase MLKL mediates necroptosis via a molecular switch mechanism. *Immunity* **39**, 443–453.
- 13 Hildebrand JM, Tanzer MC, Lucet IS, Young SN, Spall SK, Sharma P, Pierotti C, Garnier JM, Dobson RC, Webb AI *et al.* (2014) Activation of the pseudokinase MLKL unleashes the four-helix bundle domain to induce membrane localization and necroptotic cell death. *Proc Natl Acad Sci USA* **111**, 15072–15077.
- 14 Dondelinger Y, Declercq W, Montessuit S, Roelandt R, Goncalves A, Bruggeman I, Hulpiau P, Weber K, Schon CA, Marquis RW *et al.* (2014) MLKL compromises plasma membrane integrity by binding to phosphatidylinositol phosphates. *Cell Rep* **7**, 971–981.
- 15 Wang H, Sun L, Su L, Rizo J, Liu L, Wang LF, Wang FS & Wang X (2014) Mixed lineage kinase domain-like protein MLKL causes necrotic membrane disruption upon phosphorylation by RIP3. *Mol Cell* **54**, 133–146.
- 16 Zhou W & Yuan J (2014) Necroptosis in health and diseases. *Semin Cell Dev Biol* **35**, 14–23.
- 17 Dara L, Liu ZX & Kaplowitz N (2016) Questions and controversies: the role of necroptosis in liver disease. *Cell Death Discov* **5**, 16089.
- 18 Roychowdhury S, McMullen MR, Pisano SG, Liu X & Nagy LE (2013) Absence of receptor interacting protein kinase 3 prevents ethanol-induced liver injury. *Hepatology* **57**, 1773–1783.
- 19 Ramachandran A, McGill MR, Xie Y, Ni HM, Ding WX & Jaeschke H (2013) Receptor interacting protein kinase 3 is a critical early mediator of acetaminophen-induced hepatocyte necrosis in mice. *Hepatology* **58**, 2099–2210.
- 20 Gautheron J, Vucur M, Reisinger F, Cardenas DV, Roderburg C, Koppe C, Kreggenwinkel K, Schneider AT, Bartneck M, Neumann UP *et al.* (2014) A positive feedback loop between RIP3 and JNK controls non-alcoholic steatohepatitis. *EMBO Mol Med* **6**, 1062–1074.
- 21 Afonso MB, Rodrigues PM, Carvalho T, Caridade M, Borralho P, Cortez-Pinto H, Castro RE & Rodrigues CM (2015) Necroptosis is a key pathogenic event in human and experimental murine models of non-alcoholic steatohepatitis. *Clin Sci (Lond)* **129**, 721–739.
- 22 Jouan-Lanhouet S, Arshad MI, Piquet-Pellorce C, Martin-Chouly C, Le Moigne-Muller G, Van Herreweghe F, Takahashi N, Sergeant O, Lagadic-Gossmann D, Vandenabeele P *et al.* (2012) TRAIL induces necroptosis involving RIPK1/RIPK3-dependent PARP-1 activation. *Cell Death Differ* **19**, 2003–2014.
- 23 Takemoto K, Hatano E, Iwaisako K, Takeiri M, Noma N, Ohmae S, Toriguchi K, Tanabe K, Tanaka H, Seo S *et al.* (2014) Necrostatin-1 protects against reactive oxygen species (ROS)-induced hepatotoxicity in acetaminophen-induced acute liver failure. *FEBS Open Bio* **4**, 777–787.
- 24 Günther C, He GW, Kremer AE, Murphy JM, Petrie EJ, Amann K, Vandenabeele P, Linkermann A, Poremba C, Schleicher U *et al.* (2016) The pseudokinase MLKL mediates programmed hepatocellular necrosis independently of RIPK3 during hepatitis. *J Clin Invest* **126**, 4346–4360.
- 25 Filliol A, Piquet-Pellorce C, Le Seyec J, Farooq M, Genet V, Lucas-Clerc C, Bertin J, Gough PJ, Dimanche-Boitrel MT, Vandenabeele P *et al.* (2016) RIPK1 protects from TNF- α -mediated liver damage during hepatitis. *Cell Death Dis* **7**, e2462.
- 26 Li JX, Feng JM, Wang Y, Li XH, Chen XX, Su Y, Shen YY, Chen Y, Xiong B, Yang CH *et al.* (2014) The B-Raf(V600E) inhibitor dabrafenib selectively

- inhibits RIP3 and alleviates acetaminophen-induced liver injury. *Cell Death Dis* **5**, e1278.
- 27 Teng X, Degtrev A, Jagtap P, Xing X, Choi S, Denu R, Yuan J & Cuny GD (2005) Structure-activity relationship study of novel necroptosis inhibitors. *Bioorg Med Chem Lett* **15**, 5039–5044.
- 28 Takahashi N, Duprez L, Grootjans S, Cauwels A, Nerinckx W, DuHadaway JB, Goossens V, Roelandt R, Van Hauwermeiren F, Libert C *et al.* (2012) Necrostatin-1 analogues: critical issues on the specificity, activity and in vivo use in experimental disease models. *Cell Death Dis* **3**, e437.
- 29 Christofferson DE, Li Y, Hitomi J, Zhou W, Upperman C, Zhu H, Gerber SA, Gygi S & Yuan J (2012) A novel role for RIP1 kinase in mediating TNF α production. *Cell Death Dis* **3**, e320.
- 30 Harris PA, Bandyopadhyay D, Berger SB, Campobasso N, Capriotti CA, Cox JA, Dare L, Finger JN, Hoffman SJ, Kahler KM *et al.* (2013) Discovery of small molecule RIP1 kinase inhibitors for the treatment of pathologies associated with necroptosis. *ACS Med Chem Lett* **4**, 1238–1243.
- 31 Fauster A, Rebsamen M, Huber KV, Bigenzahn JW, Stukalov A, Lardeau CH, Scorzoni S, Bruckner M, Gridling M, Parapatics K *et al.* (2015) A cellular screen identifies ponatinib and pazopanib as inhibitors of necroptosis. *Cell Death Dis* **6**, e1767.
- 32 Najjar M, Suebsuwong C, Ray SS, Thapa RJ, Maki JL, Nogusa S, Shah S, Saleh D, Gough PJ, Bertin J *et al.* (2015) Structure guided design of potent and selective ponatinib-based hybrid inhibitors for RIPK1. *Cell Rep* **10**, 1850–1860.
- 33 Berger SB, Harris P, Nagilla R, Kasparcova V, Hoffman S, Swift B, Dare L, Schaeffer M, Capriotti C, Ouellette M *et al.* (2015) Characterization of GSK'963: a structurally distinct, potent and selective inhibitor of RIP1 kinase. *Cell Death Discov* **1**, 15009.
- 34 Harris PA, King BW, Bandyopadhyay D, Berger SB, Campobasso N, Capriotti CA, Cox JA, Dare L, Dong X, Finger JN *et al.* (2016) DNA-encoded library screening identifies Benzo[b][1,4]oxazepin-4-ones as highly potent and monoselective receptor interacting protein 1 kinase inhibitors. *J Med Chem* **59**, 2163–2178.
- 35 Degtrev A & Linkermann A (2016) Generation of small molecules to interfere with regulated necrosis. *Cell Mol Life Sci* **73**, 2251–2267.
- 36 Ren Y, Su Y, Sun L, He S, Meng L, Liao D, Liu X, Ma Y, Liu C, Li S *et al.* (2017) Discovery of a highly potent, selective, and metabolically stable inhibitor of receptor-interacting protein 1 (RIP1) for the treatment of systemic inflammatory response syndrome. *J Med Chem* **60**, 972–986.
- 37 Conrad M, Angeli JP, Vandenabeele P & Stockwell BR (2016) Regulated necrosis: disease relevance and therapeutic opportunities. *Nat Rev Drug Discov* **15**, 348–366.
- 38 Harris PA, Berger SB, Jeong JU, Nagilla R, Bandyopadhyay D, Campobasso N, Capriotti CA, Cox JA, Dare L, Dong X *et al.* (2017) Discovery of a First-in-Class Receptor Interacting Protein 1 (RIP1) kinase specific clinical candidate (GSK2982772) for the treatment of inflammatory diseases. *J Med Chem* **60**, 1247–1261.
- 39 Miao B & Degtrev A (2009) Methods to analyze cellular necroptosis. *Methods Mol Biol* **559**, 79–93.
- 40 Tiegs G & Gantner F (1996) Immunotoxicology of T cell-dependent experimental liver injury. *Exp Toxicol Pathol* **48**, 471–476.
- 41 Wang L, Du F & Wang X (2008) TNF-alpha induces two distinct caspase-8 activation pathways. *Cell* **133**, 693–703.
- 42 Dondelinger Y, Aguilera MA, Goossens V, Dubuisson C, Grootjans S, Dejardin E, Vandenabeele P & Bertrand MJ (2013) RIPK3 contributes to TNFR1-mediated RIPK1 kinase-dependent apoptosis in conditions of cIAP1/2 depletion or TAK1 kinase inhibition. *Cell Death Differ* **20**, 1381–1392.
- 43 Xie T, Peng W, Liu Y, Yan C, Maki J, Degtrev A, Yuan J & Shi Y (2013) Structural basis of RIP1 inhibition by necrostatins. *Structure* **21**, 493–499.
- 44 Kopalli SR, Kang TB & Koppula S (2016) Necroptosis inhibitors as therapeutic targets in inflammation mediated disorders – a review of the current literature and patents. *Expert Opin Ther Pat* **26**, 1239–1256.
- 45 Biton S & Ashkenazi A (2011) NEMO and RIP1 control cell fate in response to extensive DNA damage via TNF- α feedforward signaling. *Cell* **145**, 92–103.
- 46 Selig R, Schollmeyer D, Albrecht W & Laufer S (2011) The application of Stille cross-coupling reactions with multiple nitrogen containing heterocycles. *Tetrahedron* **67**, 9204–9213.
- 47 Bali A, Sen U & Peshin T (2014) Synthesis, docking and pharmacological evaluation of novel indole based potential atypical antipsychotics. *Eur J Med Chem* **74**, 477–490.
- 48 Fabian MA, Biggs WH 3rd, Treiber DK, Atteridge CE, Azimioara MD, Benedetti MG, Carter TA, Ciceri P, Edeen PT, Floyd M *et al.* (2005) A small molecule-kinase interaction map for clinical kinase inhibitors. *Nat Biotechnol* **23**, 329–336.

Supporting information

Additional Supporting Information may be found online in the supporting information tab for this article:

Table S1. Matrix of screen for the selectivity profiling of Sibiriline (Sib) (related to Fig. 5A).